NTNU – Trondheim
Norwegian University of
Science and Technology

Comparison of single and parallel ejector operation in transcritical R744 cycle.

Wojciech Foit

Master of Science in Engineering and ICT
Submission date: October 2012
Supervisor: Trygve Magne Eikevik, EPT

Norwegian University of Science and Technology
Department of Energy and Process Engineering

ACKNOWLEDGMENTS

I would like to thank first of all to my supervisor, Dr Armin Hafner, for giving me the opportunity to work in a pleasant atmosphere, and for a lot of good advice and ideas during my whole stay at SINTEF.

I would like to thank my Polish supervisor, Professor Janusz Skorek, who was supporting me with a lot of knowledge, especially during the last weeks of finishing this master thesis.

I could not forget to be thankful to Dr Krzysztof Banasiak, who was staying in SINTEF during my internship, for being always an expert in the topic of refrigeration, a lot of explanations and helping me to understand the theoretical problems as well as the issues which occured during the measurements on the rig.

Many thanks to SINTEF Staff members: both from the office and from the laboratory. I can not forget here to express special thanks to Gunnar Loshe, who was allways helpful in solving the technical problems on the rig. A lot of thanks to Dr Trond Andresen for his help in solving REFProp software issues.

Last not least, I want to thank my colleague Michał Palacz, for a good cooperation and company during my stay in Trondheim.

I am very grateful to everyone whom I met during these six months, and to all of you supporting me during my stay in Norway.

ABSTRACT

Ejector systems have been a field of research for many years. One of the latest topics are transcritical cycles with R744 refrigerant. The main reason of installing ejectors in that type of systems is the recovering of the pressure energy, lost in the classic cycles during the throttling processes.

The thesis consists basically of two parts, which both of consider the topic of parallel ejector operation. In the third part conclusions are presented.

The first part is a simplified feasibility study for a concept R744 cycle with three different ejector geometries working in parallel. MS Excel spreadsheet was created for general parameters calculations and for specific motive nozzles mass flow estimations.

The second part contains results of measurement procedures on the SINTEF test facility. First, single ejector operation was examined. Basing on the test results, characteristic of P2GGC ejector geometry has been created. Later on, a new module with two different geometries (P2GGC and A2CDC) working in parallel has been built on the rig. The parallel ejector operation has been examined, as well as single operation of each geometry. The results has been compared, considering the influence of each operation on the system parameters.

In the third part final conclusions are presented. Some ideas of further work are mentioned as well.

List of Figures

List of Tables

Nomenclature

m – mass flow rate, kg/s

p – pressure, bar

h – specific enthalpy, kJ/kg

s – specific entropy, kJ/kg*K

ρ – density, kg/m^3

Φ – ratio, -

η – efficiency, -

COP – coefficient of performance, -

x, y - variables

Short forms

GWP – Global Warming Potential

ODP – Ozone Depletion Potential

HDD – hard disk drive

PID – proportional-integral-derivative

3D – three-dimensional

CONTENTS

PART II

PART III

1 Aim of the Thesis

Investigation of the parallel ejectors operation is desirable, as a case never described before in the literature.

A few tasks were performed during the internship in SINTEF/NTNU laboratories and office. Feasibility study of a conceptual R744 transcritical cycle with parallel ejectors set was carried out. Full characteristics of motive nozzle and suction nozzle for single P2GGC geometry were prepared, basing on 86 obtained measurement points. Additionally main factors for P2GGC geometry were studied.

To investigate the parallel operation of two chosen geometries, namely P2GGC and A2CDC, significant changes of the rig were carried out. Parallel operation of two ejectors was tested in different simulated ambient conditions. The obtained results were compared to the single work of both of chosen ejectors, concerning the whole system work.

2 Introduction

2.1. Ejector Working Basis

A modern two-phase ejector is a device which does not consist of moving parts and allows to mix and compress two streams at the same time. Figure 1 presents the schema.

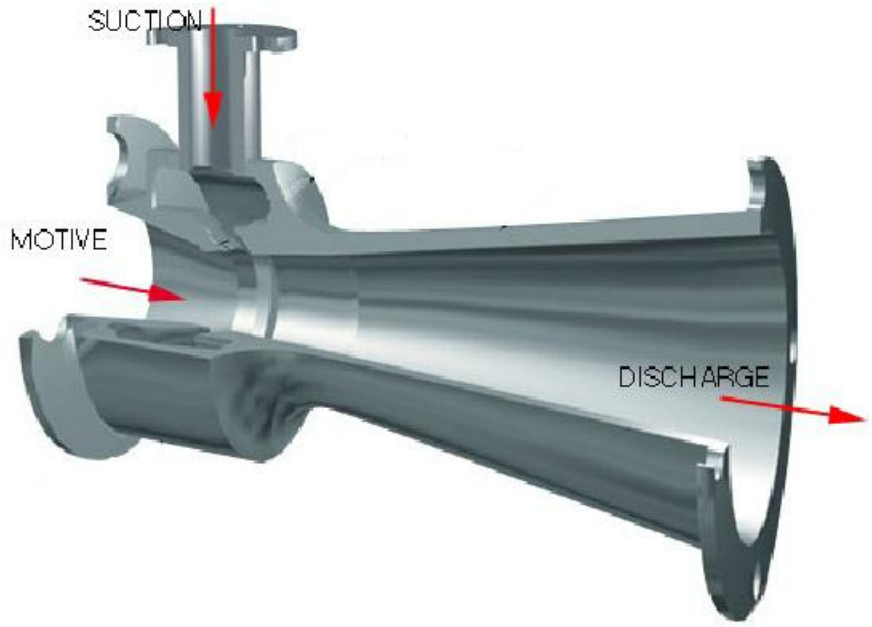

Figure 1: Schema of a two-phase ejector.

Ejector working basis is isentropic conversion of pressure into the kinetic energy. The whole process is characterized by two streams: motive and suction. The motive one is a supercritical liquid, which drives the process. It enters trough the part called motive nozzle. In motive nozzle a significant acceleration of speed as well as pressure reduction occurs. The suction flow enters by the part called suction nozzle. It is the place where suction flow is pre-accelerated for avoiding the pressure shock waves in the common area for both streams. The significantly higher pressure of motive flow causes suction of the suction flow, that appears in the part called pre-mixing chamber. The place where both flows are mixed is called mixing chamber. The mixing process is motivated by the exchange of momentum [1]. During mixing, significant shocks occur. Detailed description of the mixing process is difficult, since the motive fluid flow is described by a series of shock waves. Finally the mixed steam is directed to diffuser, where pressure increase and

speed reduction occur. It is caused by conversion of the kinetic energy of velocity to the higher level of internal energy than in the point which corresponds to suction flow input. The increased pressure in the end of diffuser is defining pressure lift – an important parameter for the ejector in specific conditions.

Because of the compression of secondary fluid from evaporator, the required work of compressor decreases, which increases more or less the system performance, the COP factor, cooling and heating capacity. Two specific factors are considered to evaluate properties of every two-phase ejector. It is: mass entrainment ratio and suction pressure ratio. The first one is a ratio of motive nozzle mass flow and suction nozzle mass flow. The second one is defined as a ratio of outlet of diffuser pressure to the pressure at the suction nozzle. Highest possible values of both mentioned ratios are desired for a well-designed ejector geometry.

2.2. Specific Parts of Ejector Geometry

Ejector parts descriptions, which are presented in this subchapter, are basing on OBRIST Engineering catalogues. The reason of that choice is further investigation of OBRIST ejectors in the rest of the thesis. Ejector parts produced by that company has the surface roughness equal to 1 micron. Figure 2 shows schema of ejector, with specific parts pointed out.

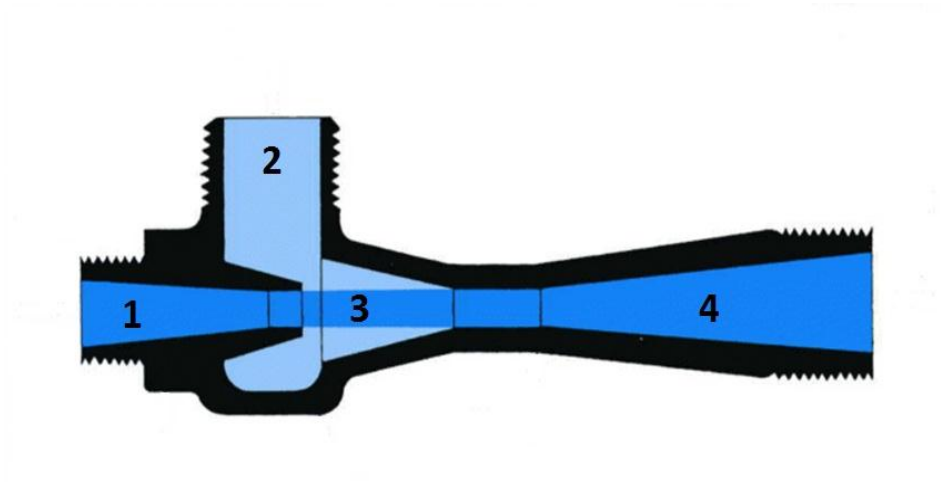

Figure 2: Schema of ejector with specific parts pointed out.
(where: 1 – motive nozzle, 2 – suction nozzle, 3 – mixing chamber, 4 – diffuser)

2.2.1. Motive Nozzle

It is the part where the high pressurized fluid enters. Motive nozzle is designed as a convergent-divergent nozzle in order to get supersonic fluid flow at the end of the nozzle outlet. The major part of that nozzle is the throat – the place where convergent part ends and divergent part begins. At this point the fluid velocity is expected to be sonic, which means that the Mach number should be equal to 1. In OBRIST motive nozzles, the convergent nozzle angle is 15° and the divergent nozzle angle could vary between 0° and 2°. Depending of the variant, throat diameter can take values from 0.7mm to 1.6 mm. The length of the divergent part could vary between 2.0mm and 8.0mm. Figure 3 shows the example of a motive nozzle.

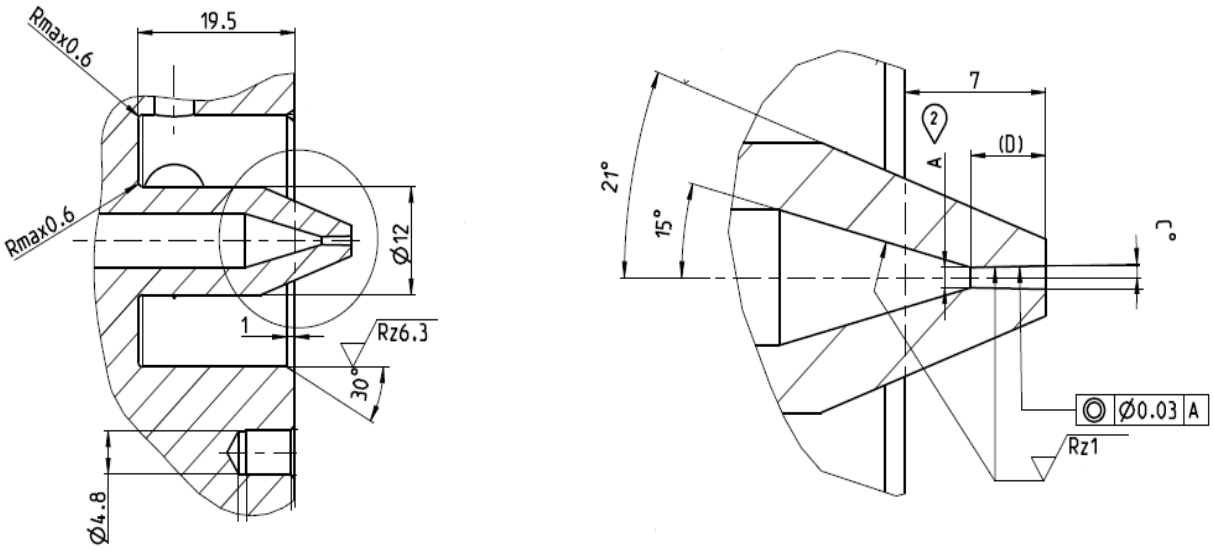

Figure 3: Technical drawings of the motive nozzle.

Because of significant difference in the velocities of motive and suction flows, the suction nozzle is needed, to accelerate the suction flow. The combination of motive nozzle and mixing chamber is forming a coaxial ring-shaped suction nozzle. Different suction nozzles can be created by mounting various distance rings between the nozzle and mixing chamber.

2.2.2. Mixing Chamber

Mixing part is designed as a straight pipe. The cone is located at the inlet, and in combination with motive nozzle creates the suction nozzle. Available OBRIST mixing chambers cones are characterized by 21° angle. The diameters could vary from 2mm to 5mm. Very important parameter is also the length of mixing chamber. To short distance of mixing chamber causes incomplete transfer of energy. When the distance is to long, energy loses can occur. Available mixing chamber lengths in OBRIST catalogue are 5xID, 10xID and 20xID. Depending on the mixing chamber size, one or two pressure sensor sockets could be prepared. Figure 4 presents the mixing chamber technical drawing.

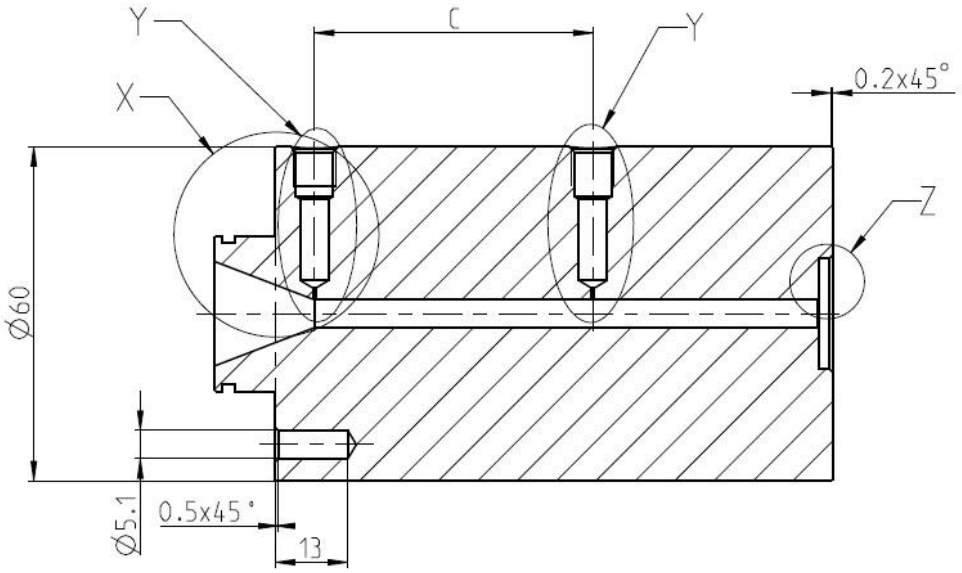

Figure 4: Technical drawing of the mixing chamber.

2.2.3. Diffuser

The diffuser is a place where the two-phase fluid is isentropically slowed down and the kinetic energy is converted in the potential energy. It causes the increase of pressure in the end of diffuser. Figure 5 shows the technical drawing of the diffuser.

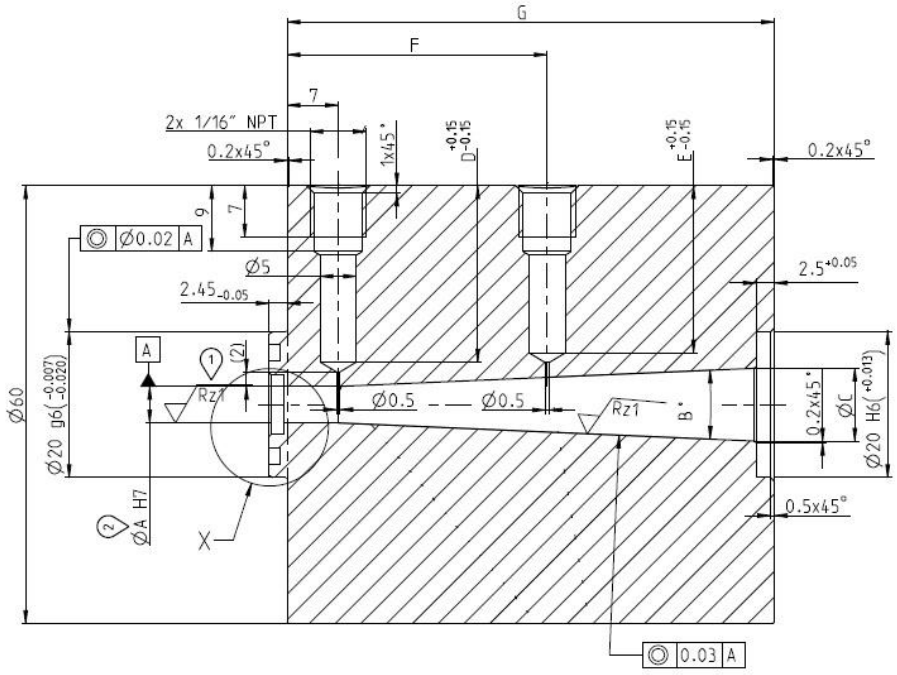

Figure 5: Technical drawing of the diffuser.

Main parameter of the diffuser is the angle. Depending on the angle two problems can be considered. In the case of small divergent angle a high pressure drop caused by friction, losses occur. For large divergent angles performance is decreasing due to boundary layer separation [2]. Among the OBRIST diffusers several diffuser angles are available. It could vary between 5° and 10°. Each diffuser has two sockets for pressure indicators prepared.

2.3. Ejector Performance Factors

As previously mentioned, two basic factors important to define the work of ejector are considered. The first one is mass entrainment ratio. According to [3] Equation (1) shows the dependence for that factor:

$$\Phi_m = \frac{\dot{m}_{evap}}{\dot{m}_{gc}} \tag{1}$$

where: $\dot{m}_{evap}$ - mass flow rate of the evaporated flow, $\dot{m}_{gc}$ - gas cooler mass flow rate.

The second factor is suction pressure ratio. Equation (2) shows the respective dependence according to [3]:

$$\Pi_s = \frac{p_{diff}}{p_{evap}} \tag{2}$$

where: p_{diff} - pressure at the diffuser outlet, p_{evap} - pressure at the evaporator outlet.

A proper-designed ejector should be characterized by high values of both factors presented above. Two extreme performances could be noticed. First is a very high pressure increment at low suction mass flow. Second is respectively small pressure increment at very high suction mass flow. None of those cases is optimal and the research for the optimal values are still desirable.

One of the significant factors is also ejector efficiency. For understanding that value, Figure 6 [4] shows the specific points in p-h diagram used in Equation (3).

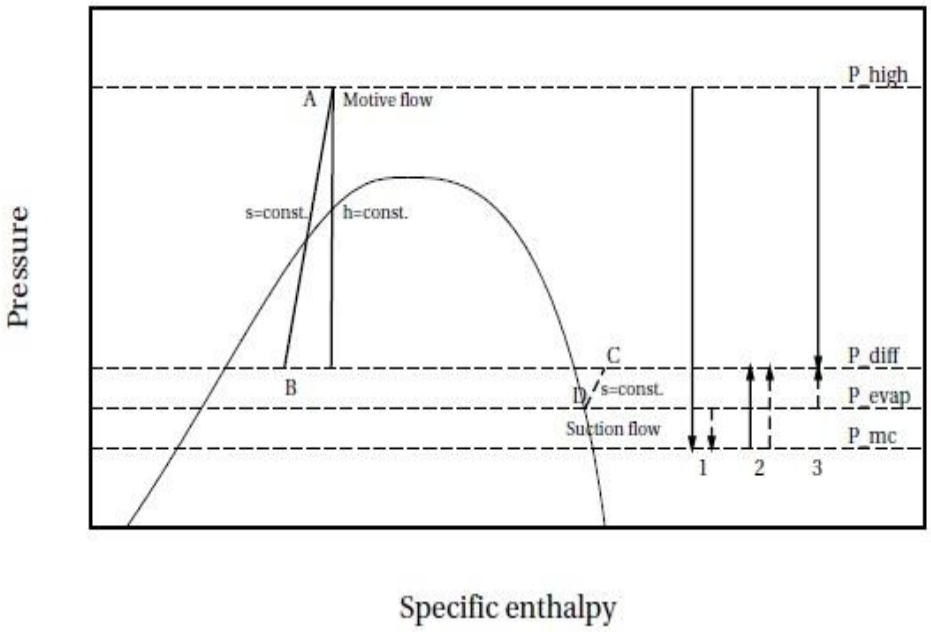

Figure 6: Processes of expansion and compression in the ejector.

Equation (3) [4, 5] presents the dependence for ejector efficiency calculation.

$$\eta_{ejec} = \Phi_m \frac{h_C - h_D}{h_A - h_B} \tag{3}$$

where: h – specific enthalpies, Φ_m - mass entrainment ratio.

2.4. Transctitical R744 Cycle

In times of fossil fuel sources decrease and global worming concern, machines driven by natural gases are desired. An example of usable natural gas is carbon dioxide, which as a refrigerant is known as R744. Some of carbon dioxide features are different, comparing to other popular refrigerants. First is the low critical temperature [6], which equals 31,1°C. The second fact is that properties of CO_2 in transcritical cycle are changing quickly, especially during temperature decrease. That requires to design a high efficient cooling heat exchanger. In every refrigeration system or heat pump cycle, the main energy losses occur in throttling process in the main throttling valve. In transcritical R744 cycle, where carbon dioxide is expanded from supercritical to subcritical state, the losses are larger than in conventional refrigerants running cycles.

To reduce that losses, ejector is installed instead of throttling valve. This change provides to several advantages. Processes in ejector are isentropicly ideal. That causes larger enthalpy differences in evaporator than in the conventional cycles. The significant advantage obtained in replacing throttling valve by ejector is compressor efficiency increase. It is because of pressure increase on the suction side, which leads to compressing unit pressure ratio decrease [7]. Figure 7 shows basic transcritical R744 cycle with installed ejector and corresponding graph with specific convertions.

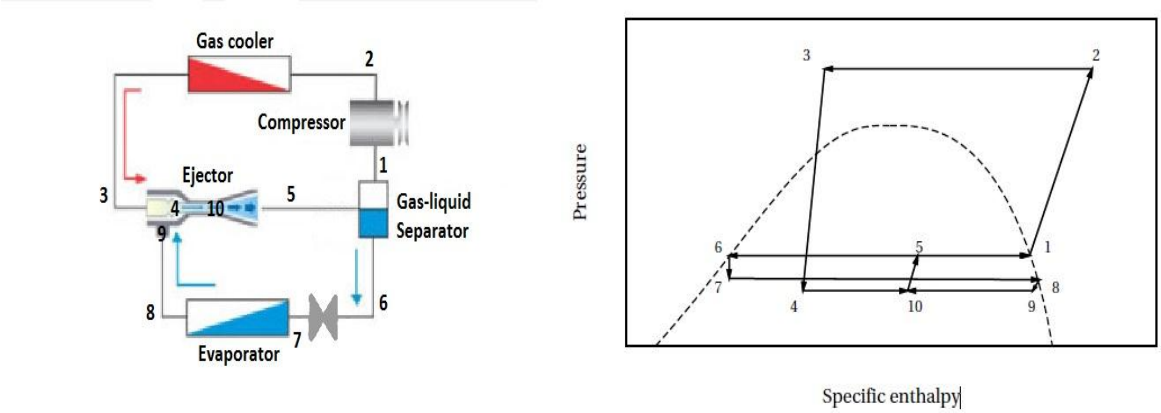

Figure 7: Diagram of transcritical R744 cycle with ejector, Corresponding graph in p-h coordinates.

The most important conversions shown on the graph in Figure 7 are:

1-2 isentropic compression in compressor

2-3 isobaric heat rejection in gas cooler

3-4 isentropic expansion in motive nozzle

4-10 isobaric mixing in mixing chamber

10-5 isentropic compression in diffuser

7-8 isobaric heat absorption in evaporator

Few challenges during the design process of transcritical CO_2 cycle should be considered. The main one is relatively high operating pressure, which may vary in some ambient conditions up to 150 bar. That leads to design a high-pressure withstand components. All of the connections and seals must withstand high pressure levels too.

2.5. Carbon Dioxide as Refrigerant

There are few specific features that refrigerants should carry out to be usable in the refrigeration systems and heat pump cycles. The main one are:

- high specific boil enthalpy
- low pressure ratio in the working temperature range
- low heat capacity for vapor and liquid form
- low normal boil temperature
- moderate vapor specific volume
- low saturation pressure in the range of condensation temperatures
- minimal value of ODP
- minimal value of GWP
- cheap costs

Among large group of refrigerants carbon dioxide (R744 in refrigerants nomenclature) is a new-discovered one. It has been used in some units over hundred years ago, but later on decommissioned due low efficiency in the high ambient temperatures [8]. Nowadays the interest in use of CO_2 increases again. It is because natural gases in the modern systems are desired. CO_2 as a refrigerant has few advantages. It is not flammable and non-toxic fluid. It is available and cheap. It can operate in vapor cycle below 0°C. R744 has ODP factor equal to 0 and minimal GWP factor, which is very important

nowadays, when the global warming discussion are running. Table 1 presents how carbon dioxide affects human body depending on the concentration in the nearest environment [9].

Table 1: Dependence between CO_2 concentration and adequate human body response.

CO_2 concentration	***Human body response***
3.3% - 5.5% for 15 minutes	Increased depth of breathing
6.5% - 7.5% for 20 minutes	Decreased mental performance
7.5%	Headaches, dizziness, disorientation
10% for 1.5 minutes	Flickering, higher muscle activity
10% for 15 minutes	Loss of consciousness
30%	Convulsions, unconsciousness

Near the critical point R744 is characterized by very good heat transfer factors. Volumetric capacity is almost 10 higher comparing to the rest of popular refrigerants. Its viscosity is low near the critical point. The relatively high operating pressures give reduction in required piping system dimensions and lower compressor displacement.

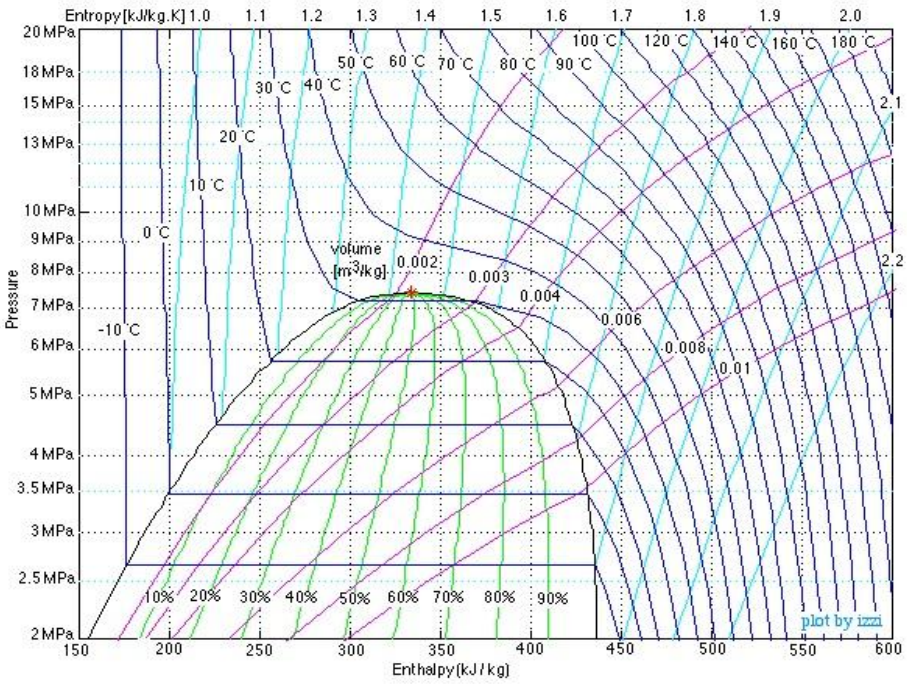

Figure 8: P-h diagram for carbon dioxide refrigerant.

PART I

3 Feasibility Study of 3-Ejector R744 Cycle

Simplified feasibility study of R744 transcritical cycle has been carried out. Fallowing chapter describes concerned cycle, shows basic calculation methods and presents the results as well as compressors set selection procedure.

3.1. Cycle Description

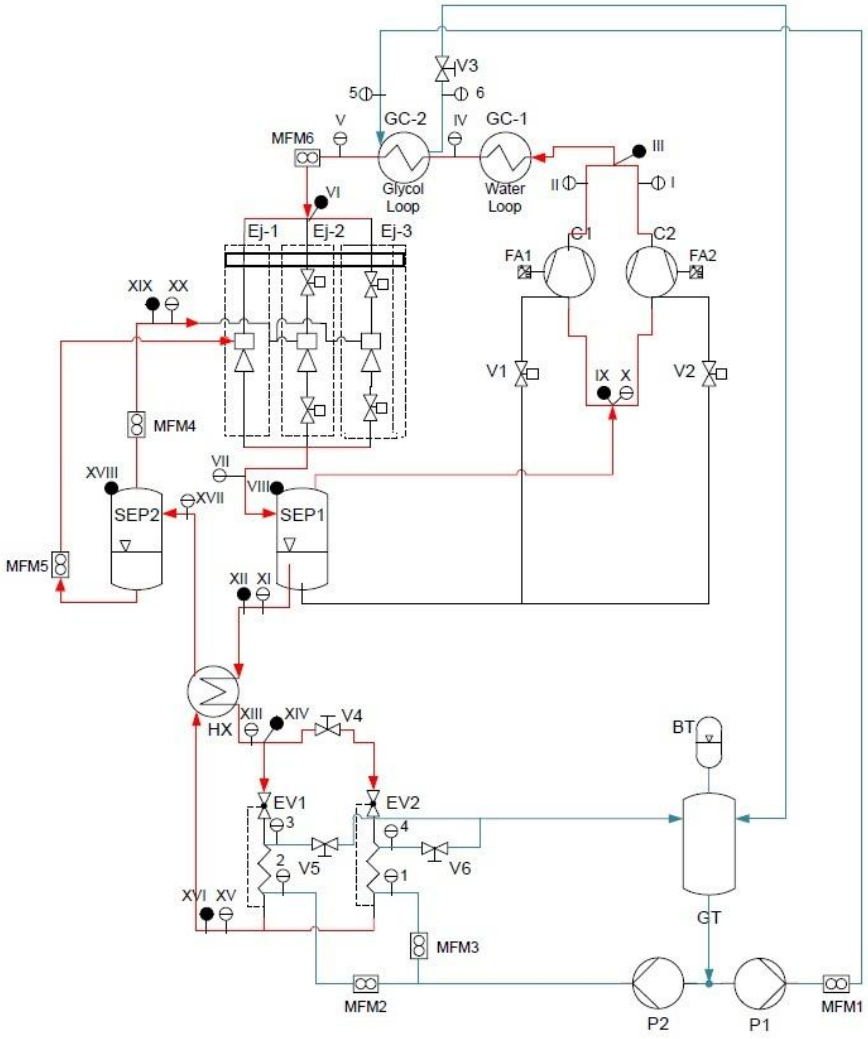

Figure 9: Concept schema of the R744 cycle with three ejectors.

A concept scheme of the designed system was created, which is shown on Figure 8. In following feasibility study just the CO_2 part (marked as red color piping) was concerned.

The basic elements of the system are:

- three ejectors (Ej-1, Ej-2, Ej-3)
- two different compressors (C1, C2)
- two gas coolers (GC-1, GC-2)
- two evaporators (EV1, EV2)
- two gas-liquid separators (SEP1, SEP2)
- one internal heat exchanger (HX)

Additionally valves (V designation), frequency adjustments (FA designation), mass flow meters (MFM designation), pressure indicators (black ones), temperature indicators (white ones) are shown on the scheme.

The system is a classic transcritical R744 refrigeration cycle with three different ejector geometries installed. However second separator is applied also, for providing liquid to suction side of the ejector characterized by the smallest motive nozzle diameter (Ej-1). Working principle of the whole system is described below.

Subcritical carbon dioxide from the main separator (SEP1) enters both of the compressors. Compressor (C1) is the main one in the cycle and it is characterized by larger volumetric displacement, comparing to compressor (C2). For the cases of higher load both compressors are running. After CO_2 is isentropically compressed to high pressure and temperature, it is directed to gas coolers. First one (GC-1) is working in the water loop and the second one (GC-2) is connected to the glycol cooling system. Heat is isobarically rejected from supercritical fluid in the gas coolers. After leaving the second gas cooler, CO_2 is directed to ejectors (Ej-1, Ej-2, Ej-3). The fluid is divided to three flows depending on the motive nozzle diameter of each ejector. Potential energy is converted to kinetic energy in each of the motive nozzles. This process causes reduction of fluid pressure and fluid velocity increases at the same time. Lower pressure field causes suction of the stream in suction nozzle. In mixing chamber both of the streams are meeting, and the process of mixing occurs. The velocities of motive stream and suction stream draw the same level. This leads to significant pressure increase. The mixed fluid is directed to the last part of ejector – diffuser. After that, each stream from the three ejectors is directed to the common collector. Cumulated stream is divided in the main separator (SEP1). Liquid phase is directed to internal heat exchanger (HX), where small temperature difference is obtained by heat exchange with fluid returning from evaporators. Next CO_2 enters evaporators (EV1 and EV2). The second evaporator (EV2) is working in cases of higher load, and is

switched on/off by a dedicated valve. After isobaric absorbtion of heat, fluid is directed to the second separator (SEP2) trough internal heat exchanger. Second gas-liquid separation ocures. Gas phase is directed to suction nozzles of second (Ej-2) and third ejector (Ej-3). Liquid CO_2 is driving suction nozzle of the smallest ejector (Ej-1).

3.2. General Calculations Methods

Thermodynamic calculations were carried out in MS Excel spreadsheet with use of functions implemented in CO2lib and REFPROP 8 libraries. All the calculations were done for R744 refrigerant and that information is not repeated in the descriptions below. However, it is an important fact for analyzing the results presented in next subchapter. In this section the main used equations are presented.

Enthalpy

Mainly the enthalpies in specific cycle points were calculated as a function of temperature and pressure, which is presented by the Equation (4):

$$h_i = f(T_i, p_i) \tag{4}$$

In case of liquid outlet from separator or liquid outlet from heat exchangers, enthalpy was calculated according to Equation (5):

$$h = f(T, p, x) \tag{5}$$

where: x – vapor quality.

Enthalpies values were calculated using CO2lib libraries.

Entropy

For compressor calculations and in few other cycle points the entropy was calculated as a function of specific enthalpy and pressure, according to Equation (6):

$$s_i = f(h_i, p_i) \tag{6}$$

Density

The density at the separator outlet was calculated by inversing the value of specific volume. Specific volume was obtained as a function of temperature and pressure (7):

$$v_i = f(t_i, p_i) \tag{7}$$

Finally density was calculated according to Equation (8):

$$\rho_i = \frac{1}{v_i} \tag{8}$$

Specific Heat

Specific heat was calculated as a function of temperature:

$$c_{p,i} = f(t_i) \tag{9}$$

Compressor

For compressors set few values were calculated, to obtain the desired parameters for choosing adequate models. The most important ones are presented below.

First one is volumetric displacement, which is given by Equation (10):

$$\dot{V} = \frac{\frac{\dot{m}}{60}}{\rho} \cdot 3600 \tag{10}$$

where: $\dot{m}$ - mass flow rate, ρ – density.

Next value is compressor efficiency, which was calculated using equation for CO_2 semi hermetic compressors according to [10]. The equation is presented below:

$$\eta_{i,C} = 1{,}1495 - 0{,}000196 \cdot n - 0{,}1036 \cdot \frac{p_2}{p_1} + 0{,}0000568 \cdot n \cdot \frac{p_2}{p_1} \tag{11}$$

where: n – compressor rotational speed, p_1 – pressure value at the compressor suction side, p_2 – pressure value at the compressor compression side.

The value of compressor efficiency was used to obtain specific enthalpy of CO_2 after compression. To perform this calculation, fallowing Equation (12) was used [11]:

$$\eta_{i,C} = \frac{h_1 - h_2}{h_1 - h_{2s}} \tag{12}$$

where: h_1 – specific enthalpy on the suction suction side, h_{2s} – specific enthalpy on for pressure value on the compression side after the ideal compression, h_2 – specific enthalpy after real compression.

Heat Exchangers

There are four (optionally five) main heat exchangers in the cycle. Two of them are working in glycol loop, one of them is working in water loop and the smallest one, namely internal heat exchanger transfers heat between two CO_2 streams.

The calculations for heat rates for evaporator as well as for the internal heat exchanger were carried out with use of classic heat transfer equation:

$$\dot{Q} = \dot{m} \cdot \left(h_{in} - h_{out} \right) \tag{13}$$

where: h_{in} - specific enthalpy at the heat exchanger inlet, h_{out} - specific enthalpy at the heat exchanger outlet.

The main gas cooler (GC-2) heat rate was calculated as the same value as the heat rate of evaporator, considering the fact that both heat exchangers are working in the same glycol loop:

$$\dot{Q}_{EV} = \dot{Q}_{GC-2} \tag{14}$$

The aggregate heat rate exchanged in both gas coolers working in the cycle was calculated using Equation (15):

$$\dot{Q}_{GC,total} = m \cdot \left(t_{C,out} - t_{GC-2,out} \right) \tag{15}$$

where: $t_{C,out}$ - temperature at the outlet of the compressors, $t_{GC-2,out}$ - temperature at the outlet of second gas cooler (GC-2).

The heat rate for the first gas cooler (GC-1) working in the water loop was calculated as the difference between the total exchanged heat rate and the heat rate of the main gas cooler (GC-2) working in the glycol loop:

$$\dot{Q}_{GC-1} = \dot{Q}_{total} - \dot{Q}_{GC-2} \tag{15}$$

where: $\dot{Q}_{total}$ - total heat rate for both gas coolers, $\dot{Q}_{GC-2}$ - heat rate of the second gas cooler working in glycol loop.

3.3. Mass Flow Rates Calculations Algorithm

There are three different ejector geometries in concerned cycle, working in parallel. Each of the geometries is characterized by specific motive nozzle diameter:

- Ejector 1 (Ej-1): 0,7 mm
- Ejector 2 (Ej-2): 0,9 mm
- Ejector 3 (Ej-3): 1,2 mm.

The motive nozzle diameter is the parameter which mainly determines the value of fluid mass flow rate which enters each ejector at motive nozzle. The value of the mass flow rate depends also strongly on the fluid parameters, namely temperature and pressure.

3.3.1. Metastable Region Theory

To understand the calculation algorithm created to obtain the mass flow rates in particular ejector motive nozzles, the metastable region theory has to be explained. Motive nozzle is a convergent-divergent nozzle, which in simplification could be presented as capillary tube. Pressure of refrigerant flowing trough an adiabatic capillary tube is decreasing. At the same time refrigerant is changing the phase. Figure 10 presents pressure and saturated pressure distributions during that process [12].

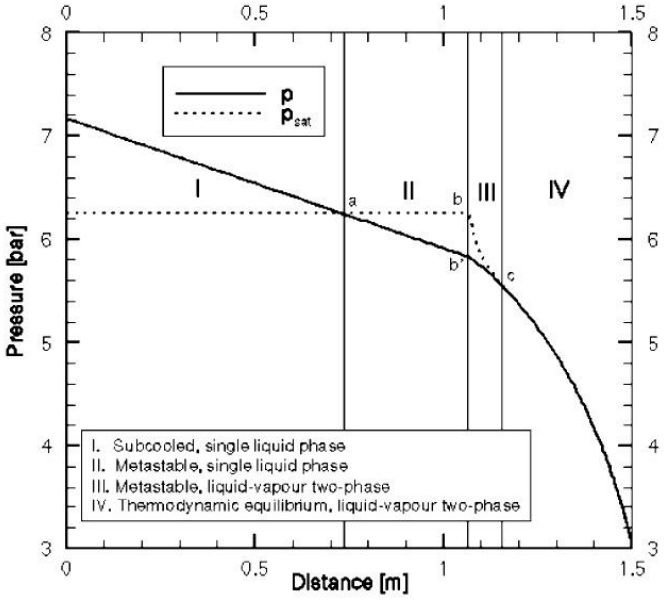

Figure 10: Pressure and saturated pressure distributions in a typical capillary tube.

There are four different regions separated during the flow [12]: subcooled region (zone I), metastable liquid region (zone II), metastable two-phase region (zone III), thermodynamic equilibrium two-phase region (zone IV). At point *a* pressure of fluid is equal to the saturation pressure but vaporization does not take place. At point *b* which is in the beginning of metastable two-phase region, the vapor bubbles appear and the pressure suddenly drops. However, this is a metaphase region because of existence of superheat liquid together with saturated liquid phase and vapor fluid phase. At passing point *c*, the thermodynamic equilibrium state is reached.

As mentioned before in the metastable two-phase region (zone III), the fluid flow can be separated into three stages: superheated liquid, saturated liquid and vapor fluid. In calculations described below, parameter *y* is an important one. It is defined as mass ratio of total saturated phase to total phase:

$$y = \frac{m_l + m_g}{m_l + m_g + m_m} \tag{16}$$

where: m_l – mass of saturated liquid, m_g – mass of vapor fluid, m_m – mass of superheat liquid.

This parameter is evaluated by correlation proposed in [13]:

$$\frac{\delta y}{\delta z} = 0{,}02 \cdot \left(\frac{P}{A}\right) \cdot (1 - y) \cdot \left[\frac{p_{sat,l} - p}{p_c - p_{sat,l}}\right]^{0,25} \tag{17}$$

where: P – capillary tube perimeter, A – cross-section area, $p_{sat,l}$ – saturation pressure of liquid phase, p_c – critical pressure of the refrigerant .

3.3.2. Calculations Algorithm

For the calculation algorithm two assumptions were considered:

- velocity value of the refrigerant that enters the motive nozzle, equals to 0 ($w_{mn,1}$=0),
- Mach Number at the end of the motive nozzle, equals to 1 (Ma=1) to obtain the sonic flow at the end of the nozzle.

There has been created a MS Excel spreadsheet, which concerns described assumptions and equations described below, to obtain the motive nozzle mass flows.

At the enter to the nozzle temperature ($T_{mn,1}$) and pressure ($p_{mn,1}$) are given, as the assumptions for considered system state. Those parameters are equal to the temperature and pressure values at the outlet of the second gas cooler (GC-2). Enthalpy at this point is calculated as:

$$h_{mn,1} = f\left(T_{mn,1}, p_{mn,1}\right) \tag{18}$$

Entropy at this point is calculated as function of temperature and enthalpy:

$$s_{mn,1} = f\left(T_{mn,1}, h_{mn,1}\right) \tag{19}$$

Enthalpy at the end of motive nozzle is calculated as a function of entropy calculated in Equation (19), and pressure at the end of the motive nozzle ($p_{mn,2}$):

$$h_{s,mn,2} = f\left(s_{mn,1}, p_{mn,2}\right) \tag{20}$$

However, at the beginning of calculation procedure value of pressure $p_{mn,2}$ could be set up as any positive random value, lower than pressure value at the enter of the nozzle. Later on, the pressure is varied by SOLVER Add-in to obtain desired values of Mach Number.

Next velocity value at the end of motive nozzle is calculated:

$$w_{mn,2} = \sqrt{2 \cdot \left(h_{mn,1} + \frac{w_{mn,1}^{\ 2}}{2} - h_{s,mn,2} \right)} \tag{21}$$

where: $w_{mn,1}$ – velocity value at the enter to the nozzle, equal to 0.

After that derivative of density after pressure is calculated as a function of three parameters, which shows Equation (22):

$$\frac{\delta \rho}{\delta p} = f\left(p_{mn,2}, h_{s,mn,2}, y\right) \tag{22}$$

where: y - mass ratio of total saturated phase to total phase (parameter described before).

In next step speed sound is calculated as:

$$a = \sqrt{\left(\frac{\delta \rho}{\delta p} \right)^{-1}} \tag{23}$$

Having speed sound value, Mach Number could be calculated from (24):

$$Ma = \frac{w_{mn,2}}{a} \tag{24}$$

At this point implemented to SOLVER conditional statement 'vary $p_{mn,2}$ until Ma=1' starts to work. All of the calculations presented before in this subchapter are repeated until the value of Mach Number is established to 1.

For Mach Number obtained at the desired level volumetric flow rate is calculated as:

$$V = \frac{\pi \cdot d_{mn}^{\ 2}}{4} \cdot w_{mn,2} \tag{25}$$

where: π – pi number, d_{mn} – motive nozzle diameter.

Finally mass flow rate is calculated as:

$$\dot{m} = \rho_{kr} \cdot \dot{V} \tag{26}$$

where: ρ_{kr} - density at the critical point.

Fallowing calculation algorithm results were compared to the results of experiments on one of considered motive nozzles, namely nozzle of (Ej-2), characterized by 0,9mm diameter. The results of experiments were maid available by the SINTEF Staff members, leading the project. Figure 11 shows a comparison of exemplary obtained calculation results and adequate experiment results.

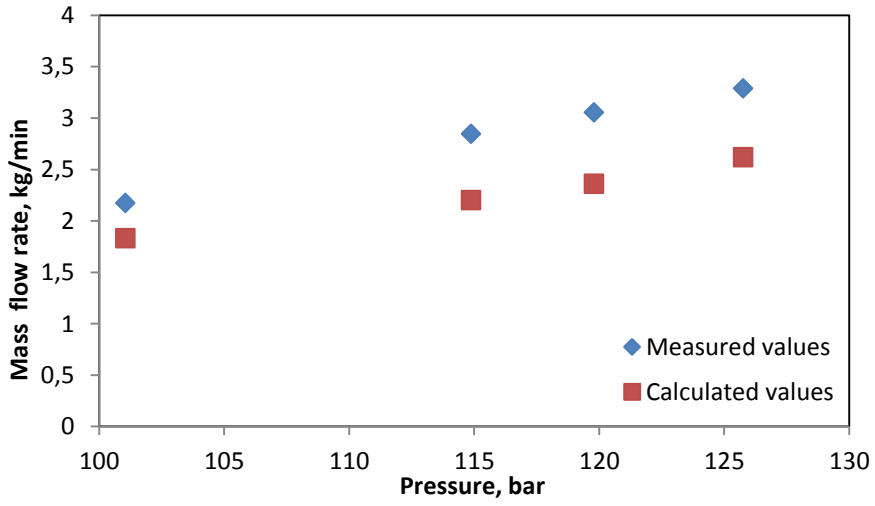

Figure 11: Comparison between calculation results and experiment results for motive nozzle mass flow rates.

3.4. Calculations Results

The results of performed study are presented in two groups. The first one consist of general results for the system. The second one presents chosen compressors set, according to the general mass flow calculations.

3.4.1. General Results

Performed calculations were carried out for three different system states. Each of them represents respectively:

- minimal operation mode
- design operation mode
- maximal operation mode

The minimal operation mode concerns only the smallest ejector (Ej-1) working. This state relates to the situation when the system is working on minimal load. The operating pressure after gas cooler (GC-2) equals to 80 bar and the temperature equals to 30°C.

The design operation mode is the typical working point for the system. All of the ejectors are in use. The operating pressure of CO_2 after the fluid exits second gas cooler (GC-2) is 80 bar and the temperature in this point equals 30°C.

Maximal operation mode is the point for high pressure and temperature conditions. In this case operating pressure of refrigerant at the entrance to ejector motive nozzle is 120 bar and the temperature equals 55°C.

For all of the cases several common assumptions were set up also. The first one is the evaporation pressure level, which equals the saturation pressure of CO_2 in temperature of -10°C. The evaporation pressure is 26,5 bar. Second assumption is related to the first one, and it states that pressure lift performed by the ejectors is 5 bar. That means the pressure of refrigerant at the outlet of ejectors equals to 31,5 bar. Third assumption constitutes that vapor quality after evaporation equals 1. Last assumption is related to temperature difference obtained in internal heat exchanger. This value equals 3K.

Table 2 is the summary of most important calculations results in respect to adequate operating mode. It contains described assumptions for each case as well as calculated specific motive nozzles mass flows, first gas cooler heat capacity, second gas cooler heat capacity, assumed volumetric displacement for compressors set, internal heat exchanger heat capacity and evaporator heat capacity.

Table 2: General calculations results for three different system states.

Value	*Minimal o.m.*	*Design o.m.*	*Maximal o.m.*
	Assumptions		
p_{GC-2}	80 bar	80 bar	120 bar
t_{GC-2}	30°C	30°C	55°C
p_{EV}	26,5 bar	26,5 bar	26,5 bar
t_{EV}	-10°C	-10°C	-10°C
p_{EJ}	31,5 bar	31,5 bar	31,5 bar
x_{EV}	1,0	1,0	1,0
ΔT_{HX}	3 K	3 K	3 K
	Calculations results		
m_{EJ-1}	0,99 kg/min	0,99 kg/min	1,31 kg/min
m_{EJ-2}	0,0 kg/min	1,53 kg/min	2,16 kg/min
m_{EJ-3}	0,0 kg/min	1,89 kg/min	2,67 kg/min
Q_{GC-1}	0,84kW	3,71 kW	11,21 kW
Q_{GC-2}	4,15 kW	18,47 kW	25,71 kW
V_C	0,71 m^3/h	3,05 m^3/h	4,25 m^3/h
Q_{HX}	0,12 kW	0,52 kW	0,72 kW
Q_{EV}	4,15 kW	18,47 kW	25,71 kW

Additionally graphic interpretation of obtained heat capacities for main heat exchangers is presented on graph shown at Figure 12.

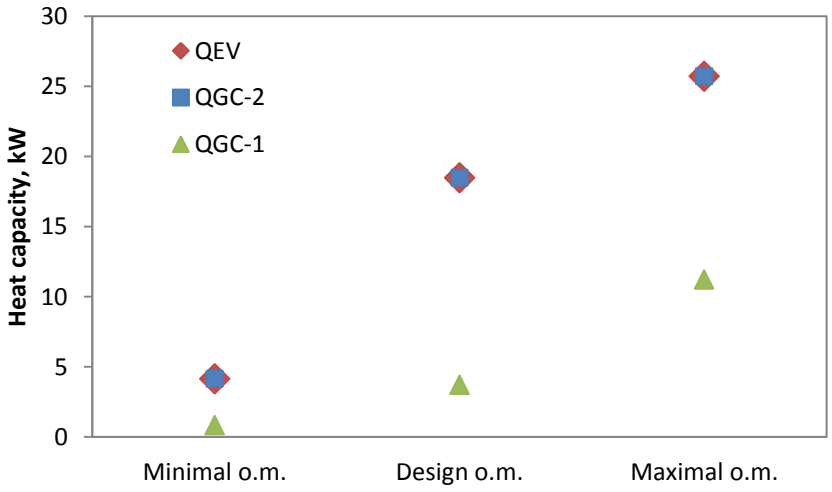

Figure 12: Heat capacities of main heat exchangers in concerned feasibility study.

3.4.2. Compressors Set Selection

For compressors set selection Dorin S.p.A. company catalogue was used. In maximal operation mode calculated volumetric displacement is 4,25 m^3/h. According to this value, two models of semi hermetic CO_2 compressors has been concerned. Each model can be connected to adequate frequency adjustment, which could vary frequencies between 35Hz and 90Hz. That gives wide changeable volumetric displacement range.

First model is Dorin CD 300M. The model comes from Dorin CO_2 semi hermetic compressors family, CD200 line. The specific volumetric displacement at frequency of 50Hz is 1,88 m^3/h. Table 3 taken from [10] shows a short specification of mentioned model.

Table 3: Basic specification of Dorin CD 300M compressor.

Description	Value
displacement 50 Hz [m3/h]	1.88
cylinders	2
oil charge [kg]	1.3
net weight [kg]	73
FLA 220-240/3/50 250-280/3/60 delta [A]	10.4
FLA 380-420/3/50 440 480/3/60 star [A]	6.0

Second compressor is the next model in Dorin CD200 compressors line – Dorin CD 350M. It is characterized by higher volumetric displacement at 50Hz than the previous model and in this case the value equals to 2,39 m^3/h. In fallowing Table 4 [10] basic specification of machine is presented.

Table 4: Basic specification of Dorin CD 350M compressor.

Description	Value
displacement 50 Hz [m3/h]	2.39
cylinders	2
oil charge [kg]	1.3
net weight [kg]	76
FLA 220-240/3/50 250-280/3/60 delta [A]	12.6
FLA 380-420/3/50 440 480/3/60 star [A]	7.3

For calculated maximal operation mode, volumetric displacement equals 4,25 m^3/h, Perfect combination of compressors in this case is connection of two Dorin CD 300M compressors. Considering average compressor efficiency at the level of 75%, this solution gives the displacement range up to 5,08 m^3/h at 90Hz. However, predicting adaptation of the system to use of other ejectors geometries which could be characterized by larger motive nozzle diameters, combination of Dorin CD 300M and Dorin CD 350M is a desired solution. It gives broader range in adjusting to system needs and still reaching calculated minimal operation mode volumetric displacement. Figure 13 presents the dependence of volumetric displacement in respect to frequency adjustment, for each described compressor as well as for two mentioned above compressors sets.

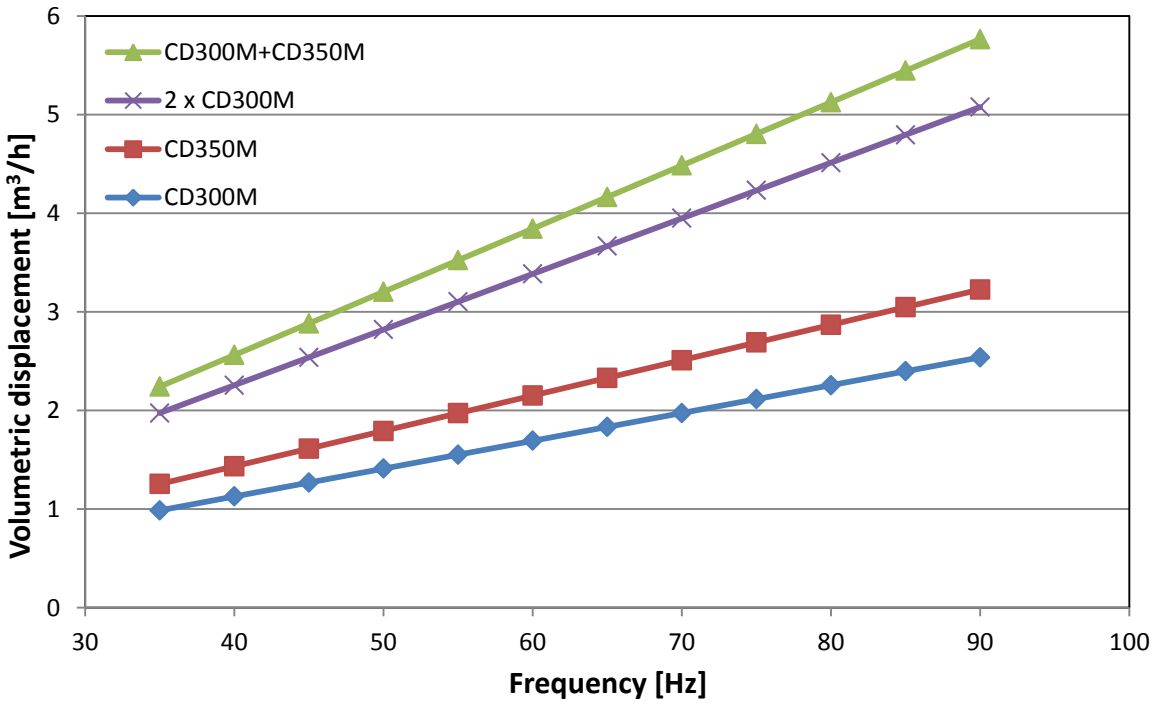

Figure 13: Dependence of volumetric displacement in respect of frequency for different compressors sets.

Finally second option has been chosen as the one which gives more flexibility and could be adapted to possible changes in the system.

PART II

4 Test Rig

Fallowing chapter contains test facility description, main parts specifications and explanation of data logging system.

The system used for running all of the experiments is placed in SINTEF/NTNU laboratory. It is built to investigate ejectors geometries in different conditions. Three types of heat exchangers are available, namely tube in tube heat exchangers, plate heat exchangers and air heat exchanger. The desired configuration could be set up by specific valves change. Both heat pump mode and cooling mode can be studied. Figure 14 shows the main part of the system.

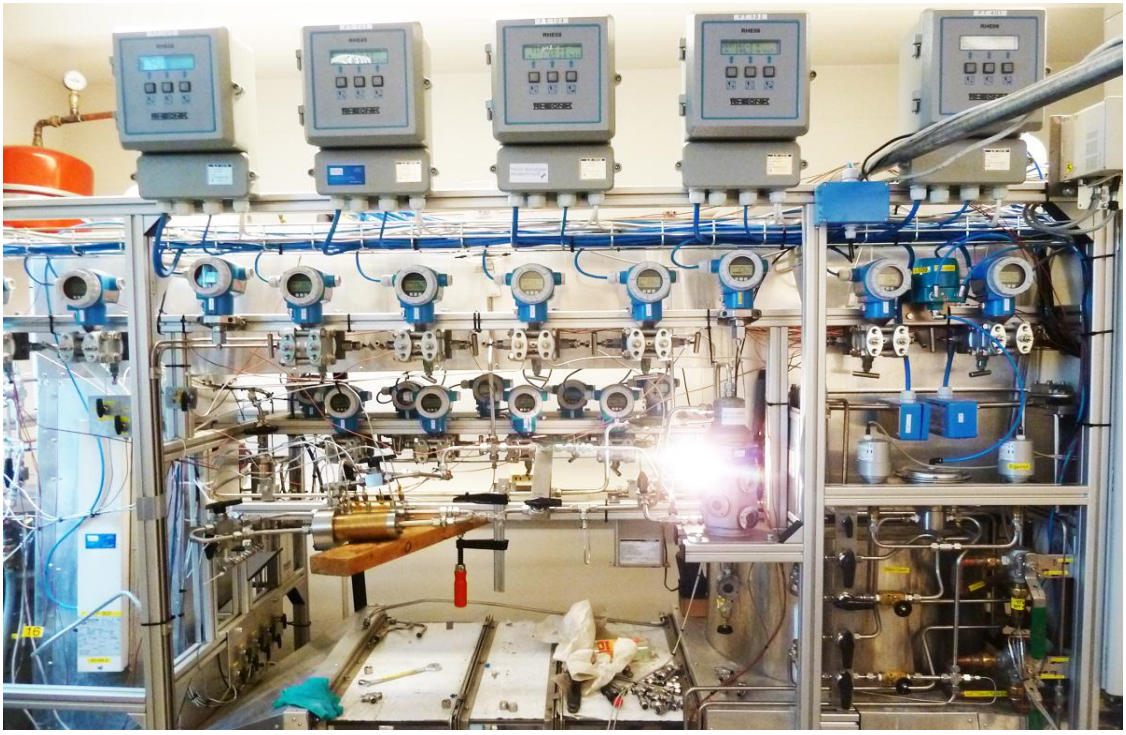

Figure 14: Photo of the main part of test facility.

4.1. Rig Schemes

Test rig scheme is presented on figure 15. Main parts of the system are shown on the scheme. Rig is working with additional cooling unit produced Swedish company Green-Cool. Cooling unit is placed in the basement of laboratory, but could be controlled from the main panel. Figure 16 presents the scheme of Green-Cool unit.

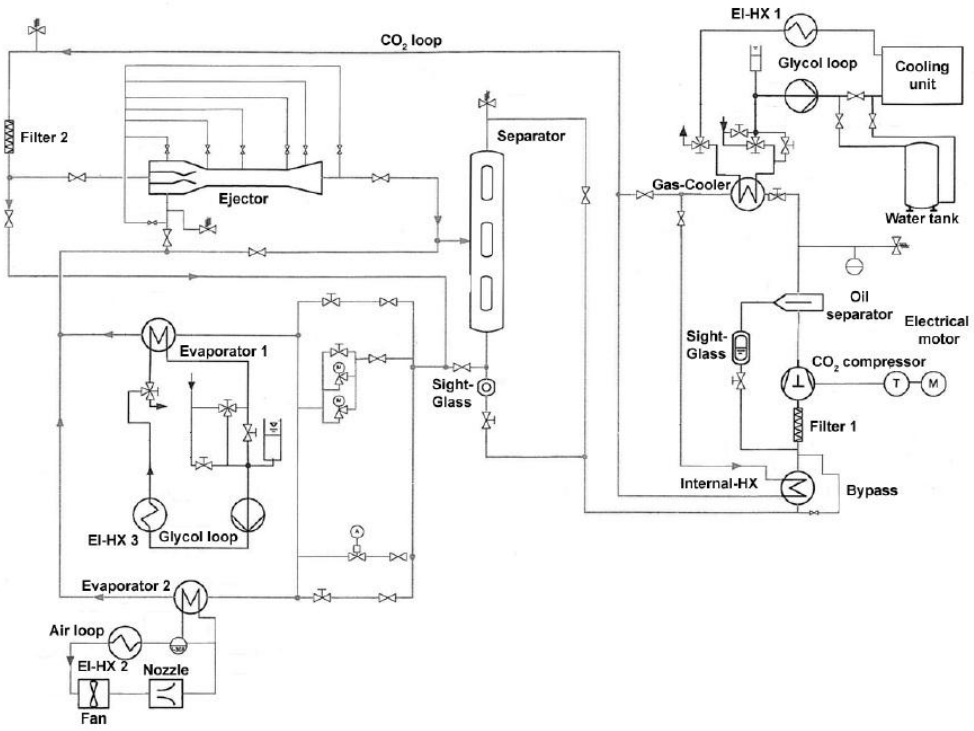

Figure 15: Scheme of SINTEF/NTNU test rig.

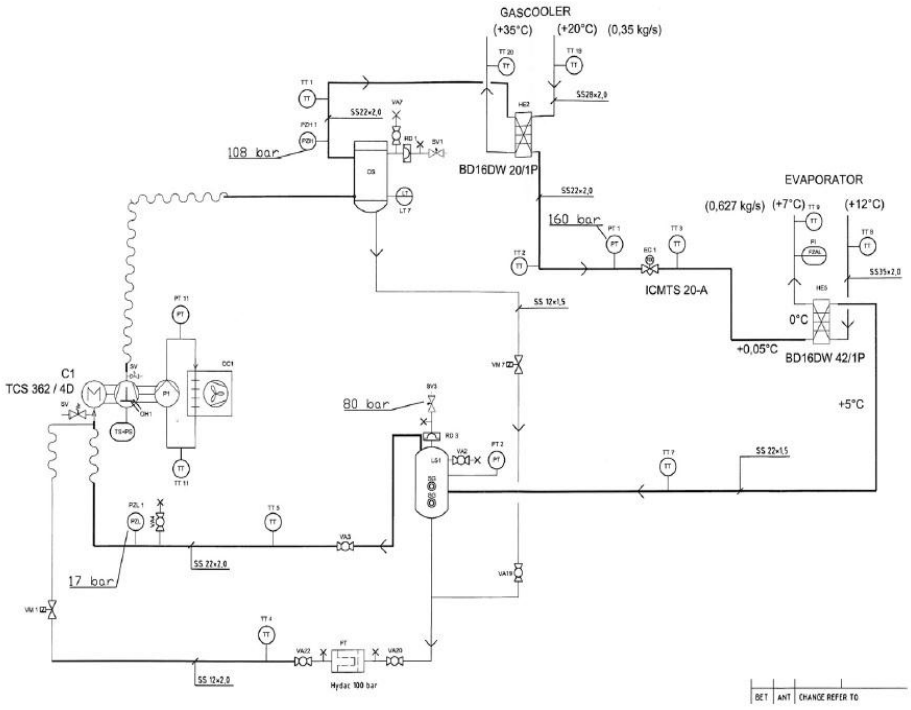

Figure 16: Green-Cool unit scheme.

4.2. Main Components

Few main rig components are described in this section, namely: separator, compressor and plate heat exchangers. Ejector, as the most important part, has been described before in Introduction chapter.

Separator

A gas-liqiud separator is required in the system. The first function is two-phase fluid separation. Separator provides also the correct amount of refrigerant in different working conditions. It is also discharging oil from the system and returning it to compressor, by dedicated throttling valve. Additional sideglass is installed below, to control the returning oil flow. Figure 17 shows gas-liquid separator with several sideglasses installed.

Figure 17: Gas-liquid separator.

Compressor

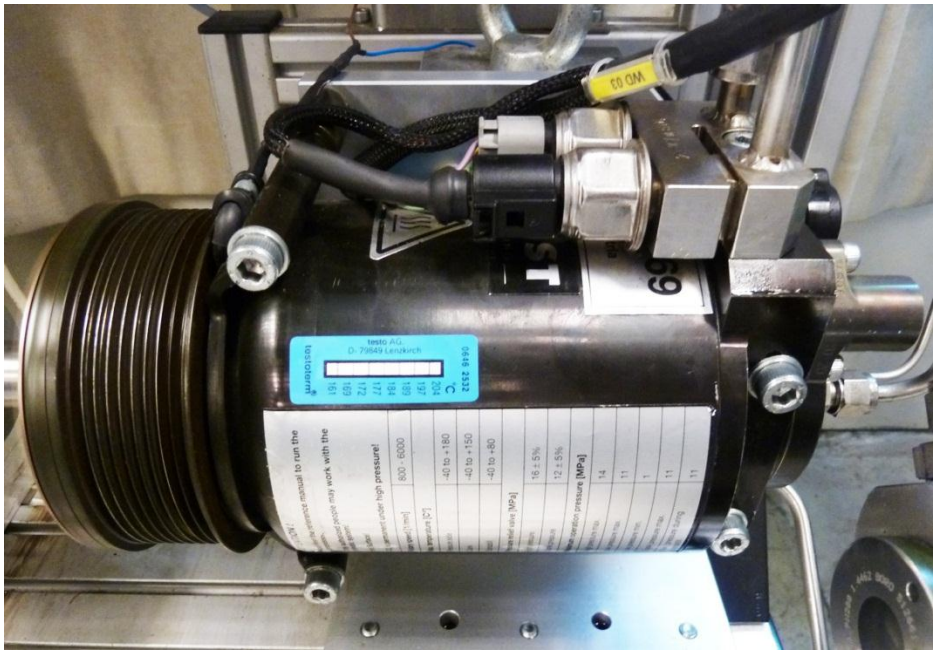

Figure 18: OBRIST C99 compressor.

Compressing unit is a reciprocating compressor. It is the C99 model produced by OBRIST Engineering. The maximum operating conditions are: 140bar and 180°C. Compressor has an additional frequency adjustment installed, which allows to choose between the speed of 800 rpm and 6000 rpm. Maximum refrigerant mass flow is 6,7 kg/s (400 kg/h). Figure 18 shows a picture of the compressor.

Plate Heat Exchangers

Evaporator as well the as gas cooler could work as tube in tube heat exchangers or plate heat exchangers. In this section plate exchangers are described.

Brazed plate exchangers installed on the rig are manufactured by KAORI company. Those type of heat exchangers have several advantages. They are: compact, small, relatively cheap, characterized by good heat transmission factors and working in high operation parameters. KAORI heat exchangers are also easy to demount and replace in the case of failure. Figure 19 shows an example of brazed plate heat exchanger [2].

Figure 19: Picture of brazed plate heat exchanger.

4.3. Measurement Devices

Few types of measurement devices installed on the rig, namely:

- mass flow meters
- temperature sensors
- pressure transmitters
- compressor controls

This subchapter describes briefly each of them, especially showing the specific uncertainties and accuracies.

Mass Flow Meters

All of the mass flow rates are measured by RHEONIK mass flow meters. The devices are working in different ranges, and for different fluids, namely: CO_2, water and oli. Every mass flow meter installed on the rig is a coriolis flow meter type. The accuracy is specified by producer to ±0,2% of reading.

Figure 20: RHEONIK mass flow meter control panel, Mass flow meter installed in CO_2 loop.

Temperature Sensors

For measuring temperatures THERMOCOAX thermocouples are used. They are Copper (Cu) / Constant (Cu-Ni), the T-type ones. Available temperature range is from -200 to 350 degree of Celsius. Producer ensures uncertainty at the level of ±0,3K for calibrated thermocouples.

Pressure Transmitters

The pressure indicators are transmitters with ceramic and silicon sensors, overload-resistant and function-monitored. The devices are manufactured by Endress+Hauser company and are characterized by long-term stability. Two types of pressure transmitters are used. Differential pressure is measured in range from -5bar to 10 bar by PMP71 sensors. The absolute pressure vary in range between 70bar and 140bar, and is measured by PDT75 sensors. The reference pressure transmitter had an accuracy of ±0.075 % of the maximum value of the scale. Figure 21 shows the absolute pressure transmitter.

Figure 21: Picture of absolute pressure indicator.

Compressor Control

There is a DMMG V2.0 detector installed between the motor and the compressor, measuring the compressor torque and compressor rotational speed. The measurement range is 0 - 50 Nm and 800 - 6000 rpm The uncertainty given by the producer of this device is ±0.25 Nm, and ±1 rpm for the rotational speed.

Fallowing Table 5 is the sum-up of the uncertainties for described indicators.

Table 5: Uncertainties values for particular indicators.

Indicator	Range	Uncertainty
Mass flow meter RHEONIK - RHM015	8 g/min to 600 g/min	±0,2 %
Mass flow meter RHEONIK - RHM04	0,2 kg/min to 10 kg/min	±0,2 %
Mass flow meter RHEONIK - RHM06	0,5 kg/min to 20 kg/min	±0,2 %
Thermocouple THERMOCOAX - Cu/CuNi	-200°C to 350°C	±0,3 K
Differential pressure transmitter Endress+Hauser - PDT75	-5 bar to 10 bar	± 0,075 of full scale
Pressure transmitter Endress+Hauser – PMP71	70 bar to 140 bar	± 0,075 of full scale
Compressor torque meter	0 Nm to 50 Nm	±0.25 Nm
Compressor rpm meter	800 rpm to 6000 rpm	±1 rpm

4.4. Data Logging Procedure

For rig controlling, changing the parameters and experimental values logging, National Instruments LabVIEW software is used. A screenshot of control panel created in LabVIEW programming environment is shown on Figure 22.

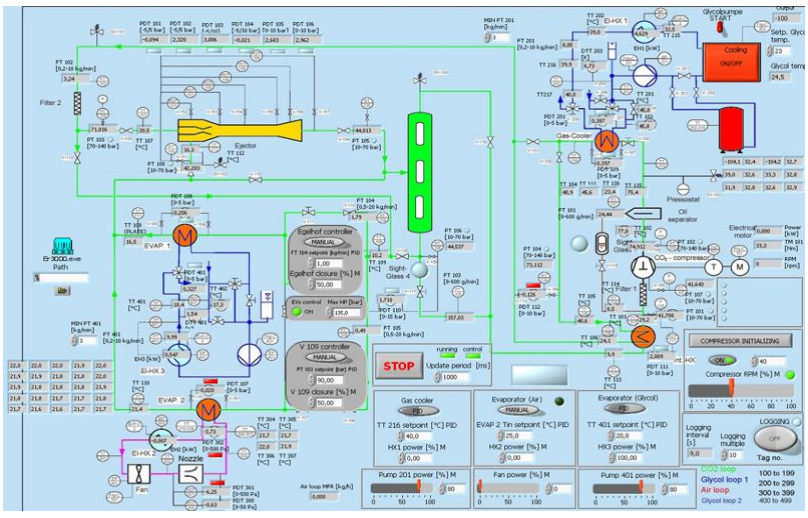

Figure 22: Test facility control panel created in NI LabVIEW.

LabVIEW as graphical type of programming environment is easy to use, which is important for researchers not being strongly familiar with programming languages. The whole method of creating new control system in LAbVIEW is dragging and dropping graphic icons, which are representing real system components. Each icon could be set up afterwards to carry out the adequate function.

Created panel of described rig is connected to the electrical enclosure, which is built on National Instruments components, basically field points. It contains also control power transformers, power disconnect and emergency stop. Field points, the main part of the enclosure, are specially programmed converters connected directly to measuring instruments. They are sending the signals to main control panel with selected time interval. The interval used for all of the measurements described in this thesis is 10 s.

Data gained by field points could be saved on computer HDD while the logging option is activated in main control panel. Afterwards values are processed in dedicated MS Excel calculation spreadsheets, which are basing on CO_2 properties libraries, such as CO2 Lib or REFPROP. Figure 23 presents the data logging procedure.

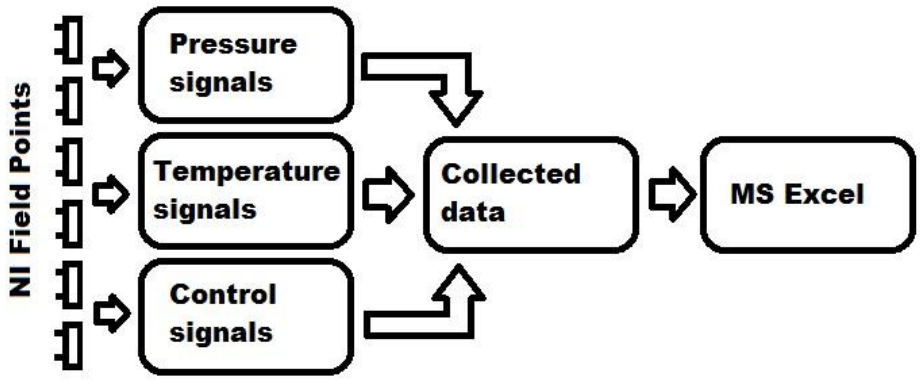

Figure 23: Schema of data logging procedure.

5 Measurement Procedures and Experiment Results

This section describes two types of experiments performed on the test rig. First one, called later Experiment I, regards to testing single ejector, namely P2GGC geometry. Second test, called later Experiment II, regards to the main topic of the thesis – testing the parallel work of ejectors. There were few system modifications done for the second test, which are described in dedicated subchapter.

5.1. Uncertainty Analysis

Before describing the tests and discussing obtained results, briefly description of uncertainty analyses is presented in fallowing section. First part of uncertainty analyses was mentioned in the previous section. It was the part which included particular uncertainties of the indicators installed in the system. This subchapter describes the second part, namely equations used for the calculations performed in MS Excel spreadsheet.

Error in uncertainty analyses is a difference between the true value and measured value. The true value is unknown. Uncertainty analyses is created to obtain the accurate measured value. There are two main types of errors: fixed and random. Fixed error depends on the accuracy of indicator and random error is an error of the precision index of a measurement.

Uncertainty analysis creates three descriptions for each result:

- overall fixed error is the root sum square of all fixed errors in the experiment,
- overall random error is produced from the data,
- overall uncertainty is calculated as the root sum square of the fixed errors and the random errors.

Overall uncertainty is presented by Equation (27):

$$\delta X = \sqrt{\left(fixed \quad error \right)^2 + \left(random \quad error \right)^2} \tag{27}$$

where: X – independent variable.

Enthalpy is one of the most frequent value calculated to obtain the final results. It is mainly given as a function of temperature and pressure. The uncertainty of the enthalpy value is:

$$\delta h_i = \sqrt{\left(\frac{\partial h_i}{\partial T_i} \cdot \delta T_i\right)^2 + \left(\frac{\partial h_i}{\partial p_i} \cdot \delta p_i\right)^2} \tag{28}$$

where: T – temperature, p - pressure.

The partial derivative terms can be calculated according to Equations (29) and (30):

$$\frac{\partial h_i}{\partial T_i} = c_{p,ref}(T_i, p_i) \tag{29}$$

where: $c_{p,ref}$ – specific heat capacity, calculated with use of REFPROP software functions.

$$\frac{\partial h_i}{\partial p_i} = \frac{h(T_i, p_i + \Delta p) - h(T_i, p_i)}{\Delta p} \tag{30}$$

where: Δp - small pressure difference which is implemented to calculate the gradient of partial derivation.

For the rest of values uncertainties are calculated in the way shown in example below. The example is performed for the COP value:

$$COP = \frac{\dot{Q}_{gc}}{P_{shaft}} \tag{31}$$

- Uncertainty of the COP value is calculated from following equation:

$$\delta COP = \sqrt{\left(\frac{\partial COP}{\partial \dot{Q}_{gc}} \cdot \delta \dot{Q}_{gc}\right)^2 + \left(\frac{\partial COP}{\partial P_{shaft}} \cdot \delta P_{shaft}\right)^2} \tag{32}$$

where the partial derivative terms can be calculated as shown in (33) and (34):

$$\frac{\partial COP}{\partial \dot{Q}_{gc}} = \frac{1}{P_{shaft}} \tag{33}$$

$$\frac{\partial COP}{\partial P_{shaft}} = -\frac{\dot{Q}_{gc}}{P_{shaft}^2} \tag{34}$$

Presented uncertainty analysis methods were created according to [14] and with help of examples shown in [2].

5.2. Experiment I

In the first experiment single ejector geometry was investigated. The aim was to create the full characteristics of investigated geometry based on the measurements, namely: characteristic of motive nozzle and characteristic of suction nozzle.

Investigated geometry was the one signed as P2GGC in OBRIST parts catalogues. Table 6 shows the main dimensions of described geometry.

Table 6: Ejector schema with P2GGC dimensions.

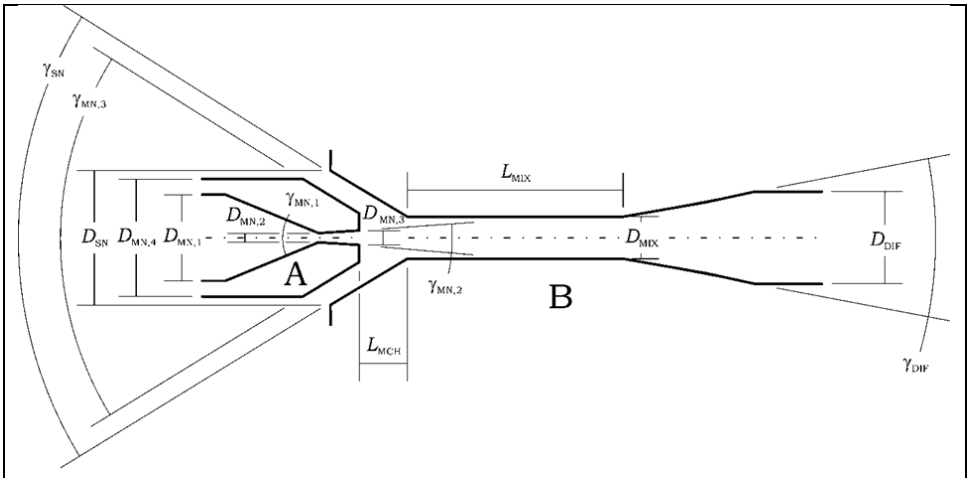

Ejector Part	Dimension	Value
Motive Nozzle	$D_{MN,1}$, mm	6
	$D_{MN,2}$, mm	1.38
	$D_{MN,3}$, mm	1.53
	$D_{MN,4}$, mm	12
	$\gamma_{MN,1}$, °	30
Pre-Mixing Chamber	L_{MCH} , mm	2.3
Mixing Chamber and Diffusor	D_{MIX} , mm	4
	L_{MIX} , mm	40
	D_{DIF} , mm	10

5.2.1. Investigation Methods for Experiment I

Before starting the investigation, ejector parts were connected with dedicated screws and all of the indicator ports were isolated with special Teflon tape. After preparing the ejector to work, it was installed in the system. Next step was filling the installation with CO2 and checking all of the connections with water with soap. This procedure was necessary to find the leaks in the system, because it was not in use for six months. After ensuring that the whole system is tight, the installation was filled again and the system was started for the tests.

To obtain different measurement results, few system settings were changed. Most tests were obtained by changing the compressor speed for steady levels of gas cooler and evaporator temperatures, with 5K superheat of evaporated gas. Superheat was obtained by regulation of installed valve. After whole compressor speed range was investigated for chosen temperature levels, or the evaporation pressure has reached the level under 34bar, new temperature levels on both heat exchangers were chosen and next series of measurements was performed.

5.2.2. General Issues During the Measurement Process

Several issues occured during all tests performed on the rig. Most of them appeared during this part of experiments and they are described just in fallowing subsection, with briefly descriptions of performed fixing solutions. The main issues were:

- Leaks in the system: after a long term investigations, leaks in the system occurred. They were noticed by decreased pressure level especially after weekend brakes in measuring. To detect them water with soap was used and detected spots were tighten by closing the leaking connections.
- Damaged O-ring in the oil filter: after first month of investigations, a leakage in the main oil filter was detected. For fixing it, new O-rings for the filter were ordered and later on the damaged O-ring was replaced by a new one.
- Damaged main closing valve: after two months of tests, significant leakage in the main valve used for CO_2 releasing was detected. Due the lack of spare valves in the laboratory, this valve was replaced by a special cap. However it is a temporary solution which should be fixed in the future.
- Floating temperature level at the gas cooler heat source setpoint: during all of the measurements temperature level set at the gas cooler heat source was adjusted on

desired level. The issue was to maintain the chosen level for the whole logging process which for the single measurement was 18 minutes. Significantly high temperature changes were causing pressure changes at the inlet to the motive nozzle. Several changes in controlling LabVIEW panel were done. Especially the variables for PID controllers, which are responsible for maintaining the temperature level were changed, namely: proportional gain, integral time and derivative time. None of this operations helped to maintain the temperature level on a stable level. This issue was described also in the thesises based on measurements performed on the same rig by Adamowicz [2] and Jurkowski [15]. Figure 24 shows the fluctuations of temperature during random measurement.

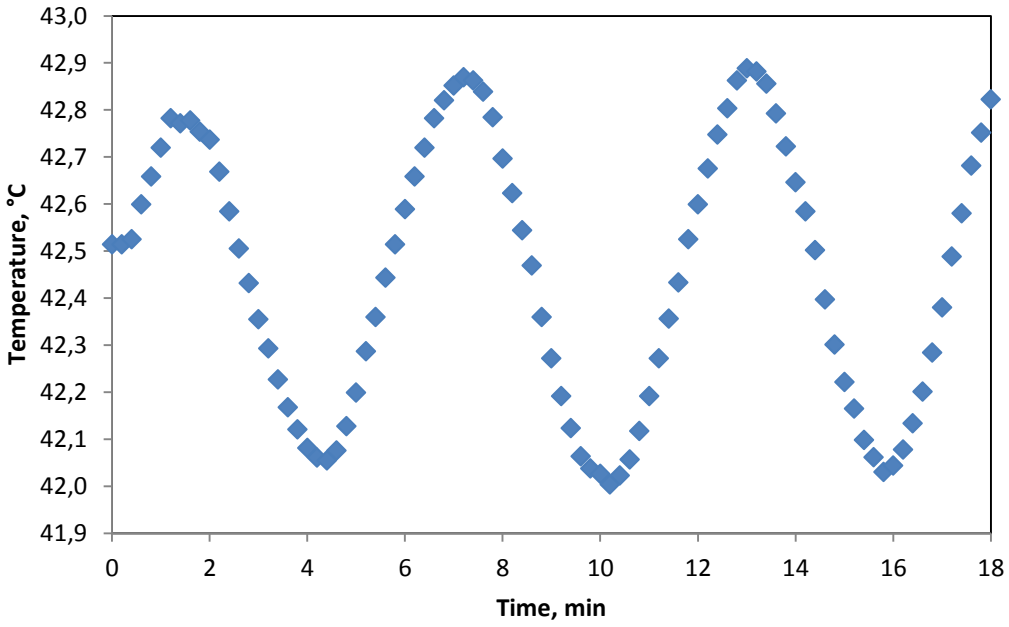

Figure 24: Temperature fluctuations for the gas cooler heat source set up on temperature level of 42,5°C.

- Compressor damage: the crucial issue during performed measurements was compressor breakdown. The reason of OBRIST C-99 compressor damage was fatigued wobble plate in the machine. This damage could not be fixed in SINTEF laboratories. Compressor was sent to the OBRIST headquarters in Austria. Fixing process took over 3 weeks. In this period, measurements were not performed.
- FT-102 mass flow meter errors: very important value measured during all of the tests was the mass flow rate at the inlet to the motive nozzle. It was measured by RHEONIK mass flow meter, marked as FT-102. Errors were displayed on the mass

flow meter control panel around twenty times during the whole measurement process. In the error state mass flow was not measured. This issue was always fixed by checking the connections between the sensor and National Instruments pick up panel or resetting the device. However, this solution is temporary and the errors may occur any time during next tests. Mass flow meter should be sent for service to the producer.

5.2.3. Procedure of Ejector Characteristics Obtaining

The first step was collecting respectively wide group of measurements. The idea was to obtain 120 measurement points in a range of motive nozzle pressures between 70 bar and 120bar. Finally 86 measurements were obtained for P2GGC geometry. Basing on this database two characteristics were prepared. First one is a characteristic of tested motive nozzle. Second characteristic is related both to motive and suction nozzle. However, it could be called the characteristic of suction nozzle.

Motive nozzle characteristic

First step of preparing the characteristic was to calculate α factor for every measurement point. A was defined as ratio of obtained motive nozzle mass flow rate, and calculated motive nozzle mass flow:

$$\alpha = \frac{\dot{m}_{mn}}{\dot{m}_{mn,calc}} \tag{35}$$

where: $\dot{m}_{mn}$ - motive nozzle mass flow rate, obtained in the measurement, $\dot{m}_{mn,calc}$ - motive nozzle mass flow rate, obtained in calculations.

The calculation method of motive nozzle mass flow rate was the same as presented in the subchapter 3.3.2., therefore it is not presented in this section.

Calculated α factors were later displayed in 3D coordinate system, with help of GoldenSoftware GRAPHER 9. Horizontal axes were presenting reduced pressure and reduced density values, and vertical axis was presenting obtained α factors. Analyzing the points correlation in such created 3D coordinate system, second function was created. It was called α_{app}, which is a function of two variables obtained in every measurement, namely motive nozzle reduced pressure and motive nozzle reduced density:

$$\alpha_{app} = f\left(p_r, \rho_{r,mn}\right) \tag{36}$$

where: p_r – motive nozzle reduced pressure, which is a ratio between motive nozzle pressure and the pressure of CO_2 at the critical point, $\rho_{r,mn}$ – motive nozzle reduced density, which is a ratio of density for motive nozzle fluid and density of CO_2 at critical point.

To obtain the proper function form, SOLVER Ad-in in MS Excel spreadsheet was used. Considering points correlation obtained in GRAPHER and studying two-variables functions formulas in mathematical charts, a function formula was found. General formula is presented in Equation (37):

$$f(x,y) = \frac{x \cdot y}{x^2 + y^2} \tag{37}$$

where: x, y –variables.

However, final version of the function was:

$$\alpha_{app} = f\left(p_r, q_{r,mn}\right) = \frac{p_r \cdot \rho_{r,mn}}{\left(\left(p_r^A - B\right)^2\right)^C + \left(\left(\rho_{r,mn}^D - E\right)^2\right)^F \cdot \left(G + H \cdot p_r^I\right)} \tag{38}$$

where: A-I – calculated in next step function coefficients.

In next step one condition was implemented in the SOLVER Ad-in. Program was searching for this A - I coefficients values, which will give the R^2 correlation coefficient of α and α_{app} values, on the level closest to 1. The highest R^2 value, namely 0,935, was found for the function presented by Equation (39):

$$f\left(p_r, q_{r,mn}\right) = \frac{p_r \cdot \rho_{r,mn}}{\left(\left(p_r^{0,051} - 0{,}997\right)^2\right)^{0,053} + \left(\left(\rho_{r,mn}^{0,361} - 0{,}858\right)^2\right)^{0,624} \cdot \left(3{,}175 + 0{,}852 \cdot p_r^{4,168}\right)} \tag{39}$$

Suction nozzle characteristic

Characteristic of ejector suction nozzle was prepared as ejector efficiency characteristic. The reason of choosing this way of interpretation was that efficiency characteristic is more practical in further use. Also knowing the efficiency, the value of suction mass flow can be obtained.

In first step efficiency was calculated for all of the measurements from the classic ejector efficiency equation, presented in Introduction chapter:

$$\eta_{ejec} = \Phi_m \frac{h_C - h_D}{h_A - h_B} \tag{40}$$

Meaning of specific enthalpies presented in Equation (40) is described in subchapter 2.3.

In the next step second function was created. It was called $\eta_{ejec,\,app}$. It is a function of one variable, namely: Π_s – suction pressure ratio, described in the subchapter 2.3. The basic formula is presented by Equation (41):

$$\eta_{ejec,app} = f(\Pi_s) = A \cdot (\Pi_s - 1)^2 + B \cdot (\Pi_s - 1) \tag{41}$$

However, A and B coefficients were calculated as two different subfunctions of three variables each, presented by Equations (42) and (43):

$$A = a_1 \cdot p_r^2 + a_2 \cdot p_r + a_3 \cdot \rho_{r,mn}^2 + a_4 \cdot \rho_{r,mn} + a_5 + a_6 \cdot \rho_{r,sn}^2 + a_7 \cdot \rho_{r,sn} \tag{42}$$

where: $a_1 – a_7$ – coefficients obtained in next step, p_r – motive nozzle reduced pressure, which is a ratio between motive nozzle pressure and the pressure of CO_2 at the critical point, $\rho_{r,mn}$ – motive nozzle reduced density, which is a ratio of density for motive nozzle fluid and density of CO_2 at critical point, $\rho_{r,sn}$ – suction nozzle reduced density, which is a ratio of density for suction nozzle fluid and density of CO_2 at critical point.

$$B = b_1 \cdot p_r^2 + b_2 \cdot p_r + b_3 \cdot \rho_{r,mn}^2 + b_4 \cdot \rho_{r,mn} + b_5 + b_6 \cdot \rho_{r,sn}^2 + b_7 \cdot \rho_{r,sn} \tag{43}$$

where: $b_1 – b_7$ – coefficients obtained in next step, p_r – motive nozzle reduced pressure, which is a ratio between motive nozzle pressure and the pressure of CO_2 at the critical point, $\rho_{r,mn}$ – motive nozzle reduced density, which is a ratio of density for motive nozzle fluid and density of CO_2 at critical point, $\rho_{r,sn}$ – suction nozzle reduced density, which is a ratio of density for suction nozzle fluid and density of CO_2 at critical point.

In last step a condition was implemented in the SOLVER Ad-in. Program was searching for this $a_1 – a_7$ and $b_1 – b_7$ coefficients values, which will give the R^2 correlation

coefficient of η_{ejec} and $\eta_{ejec,\ app}$ values, on the level closest to 1. The highest R^2 value, namely 0,906, was found for the subfunctions presented by Equations (44) and (45):

$$A = -33{,}8 \cdot p_r^2 + 96{,}3 \cdot p_r + 25{,}7 \cdot \rho_{r,mn}^2 - 61{,}2 \cdot \rho_{r,mn} - 125{,}8 - 321{,}7 \cdot \rho_{r,sn}^2 + 345{,}2 \cdot \rho_{r,sn} \quad (44)$$

$$B = 6{,}3 \cdot p_r^2 - 19{,}8 \cdot p_r - 1{,}3 \cdot \rho_{r,mn}^2 + 5{,}9 \cdot \rho_{r,mn} + 13{,}9 + 20{,}6 \cdot \rho_{r,sn}^2 - 16{,}1 \cdot \rho_{r,sn} \quad (45)$$

5.2.4. P2GGC Geometry Investigation

Analyzing obtained 86 measurement points for P2GGC geometry, few graphs were prepared to show the dependence of main ejector factors, in respect to motive nozzle conditions.

The first dependence, shown on Figure 25 is the dependence of mass entrainment ratio, marked in Introduction chapter as Φ_m, in respect to changes of motive nozzle pressure.

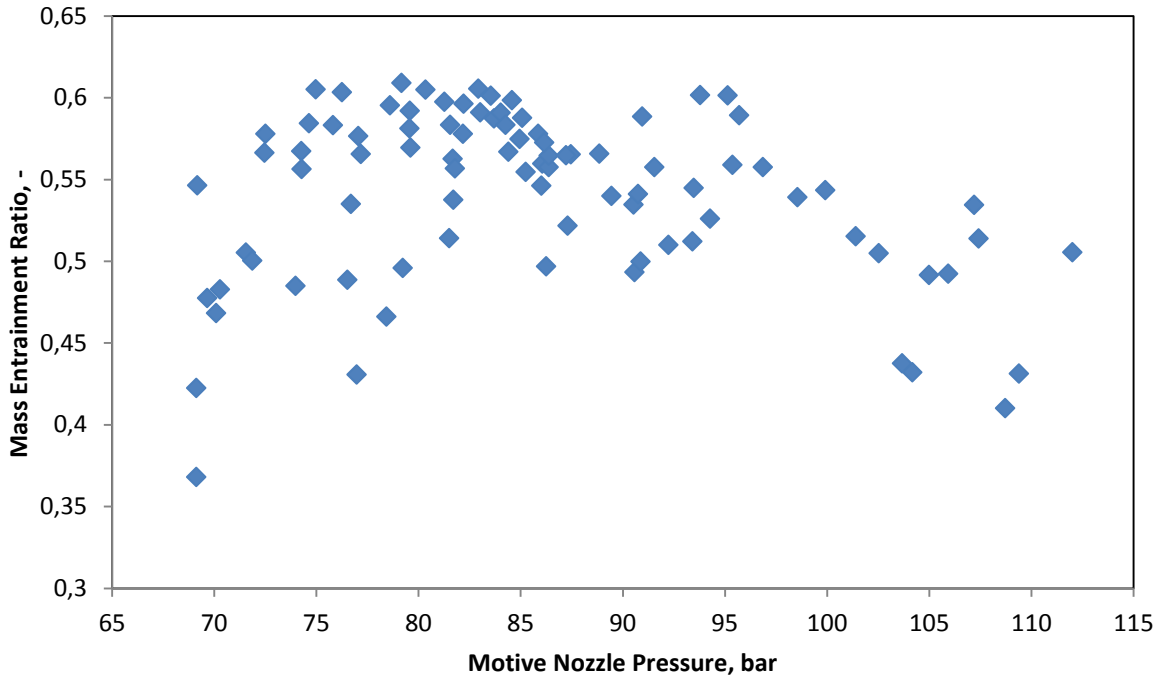

Figure 25: Dependence of mass entrainment ratio in respect to motive nozzle pressure for P2GGC geometry.

As mentioned in Introduction chapter, a well-designed ejector should be characterized by high values of mass entrainment ratio. However, there are motive nozzle pressures which give the highest and the lowest values of mass entrainment ratio. Analyzing the graph for P2GGC geometry, the highest values are obtained for 85 bar and 95 bar, and the lowest are obtained for 69 bar and 109 bar.

Next graph shown on Figure 26 presents the dependence of suction pressure ratio, marked in Introduction chapter as Π_s, in respect to the motive nozzle pressure.

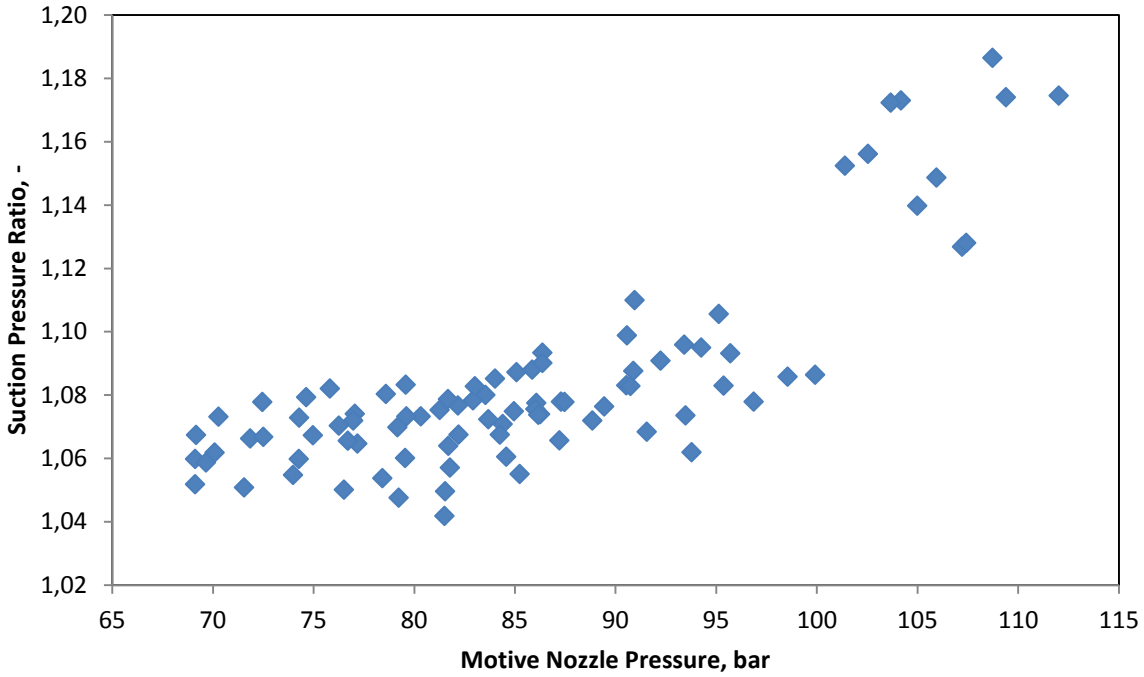

Figure 26: Dependence of suction pressure ratio in respect to motive nozzle pressure for P2GGC geometry.

A well-designed ejector should be characterized also by high values of suction pressure ratio. For some motive nozzle pressures very high values of mass entrainment ratios are obtained. For P2GGC geometry the highest values are obtained mainly for motive nozzle pressures between 103 bar and 113 bar.

Important value for ejector work is also pressure lift. It is saying what is the pressure difference between suction nozzle pressure and pressure at the diffuser outlet. Pressure lift is the main effect obtained by using ejector instead of a valve. Figure 27 presents the dependence of pressure lift in respect of motive nozzle pressure.

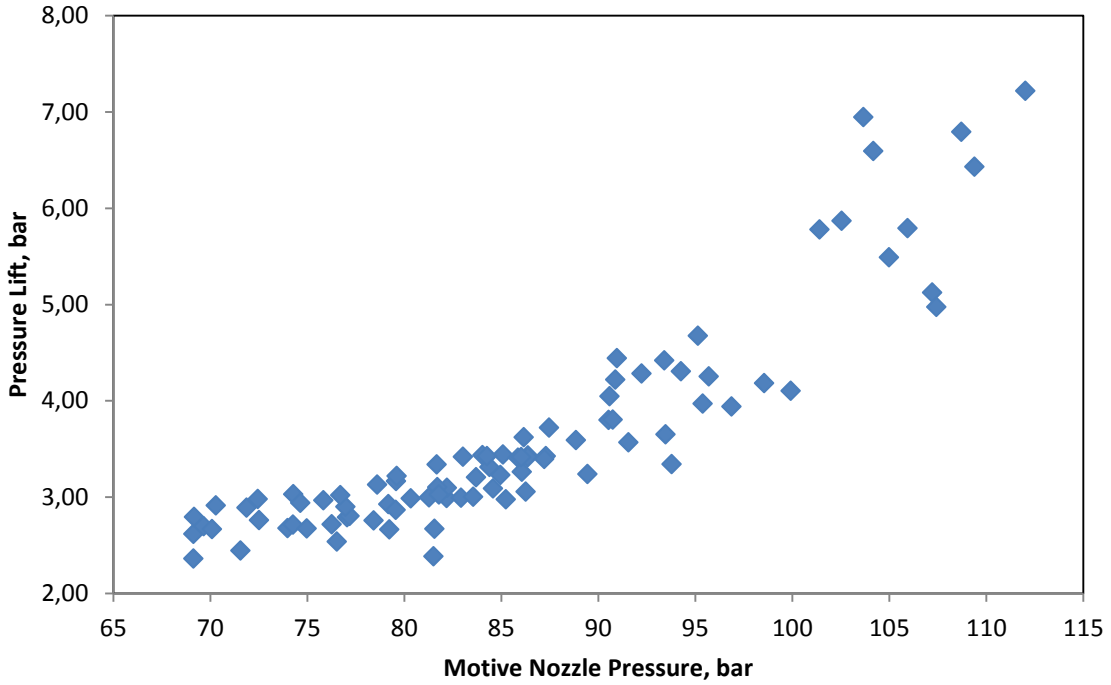

Figure 27: Dependence of pressure lift in respect to motive nozzle pressure for P2GGC geometry.

For higher motive nozzle pressures, higher pressure lifts are obtained.

The last important factor is ejector efficiency. The highest efficiency for P2GGC geometry is obtained for 91 bar, which is presented on Figure 28.

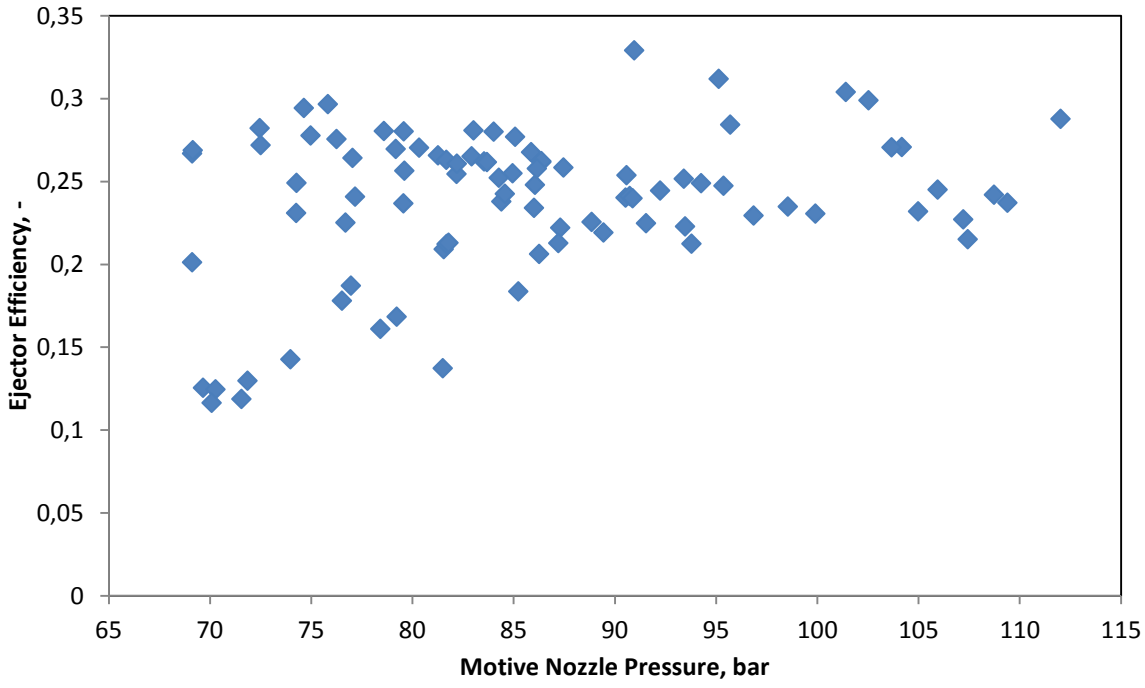

Figure 28: Dependence of ejector efficiency in respect to motive nozzle pressure for P2GGC geometry.

5.3. Experiment II

The aim of second stage of experimental tests performed on described test rig, was investigation of parallel ejectors operation. Two different geometries were chosen to investigate the effects of their common work. The first geometry is ejector signed as P2GGC, which is the same as investigated in first stage of experiment. The second geometry was chosen as the one characterized by smaller motive nozzle diameter. This choice was supported by the fact, that first geometry operation in the system was covering more than half of maximal compressor displacement. Providing, that total mass flow rate of two ejectors working in parallel is a sum of two different mass flow rates, the second geometry has to be characterized by smaller motive nozzle diameter. Considering this assumption, second geometry was chosen as the one signed in catalogue as A2CDC. Table 7 shows the basic scheme of ejector and compares the dimensions of both geometries chosen for the test.

Table 7: Ejector scheme with comparison of selected dimensions for P2GGC and A2CDC geometries.

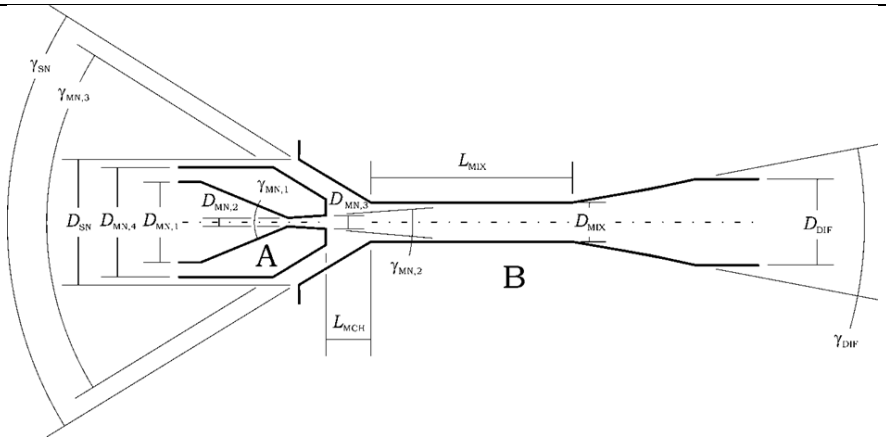

Ejector Part	Dimension	Value for P2GGC	Value for A2CDC
Motive Nozzle	$D_{MN,1}$, mm	6	6
	$D_{MN,2}$, mm	1.40	0.90
	$D_{MN,3}$, mm	1.53	1.03
	$D_{MN,4}$, mm	12	12
	$\gamma_{MN,1}$, °	30	30
Pre-Mixing Chamber	L_{MCH} , mm	2.3	1.9
Mixing Chamber and Diffusor	D_{MIX} , mm	4	3
	L_{MIX} , mm	40	15
	D_{DIF} , mm	10	10

To investigate parallel work, part of the system was modified. New pipe connections as well as several valves were installed. Mainly the modifications touched two points near the ejector. The motive nozzle line, which supplies the refrigerant from gas cooler to ejectors motive nozzle, was splitted in two lines. The same modification was performed for the suction line, which provides CO_2 from evaporator to ejectors suction nozzle. Both of those changes were done to connect the second ejector. Additionally two valves were installed to shut-off one of the ejectors optionally. In the end the discharge lines were connected to one collector line, which provides CO_2 to the gas-liquid separator. For the time of performing described modifications, the refrigerant was released from the system. Figure 29 presents part of performed modifications.

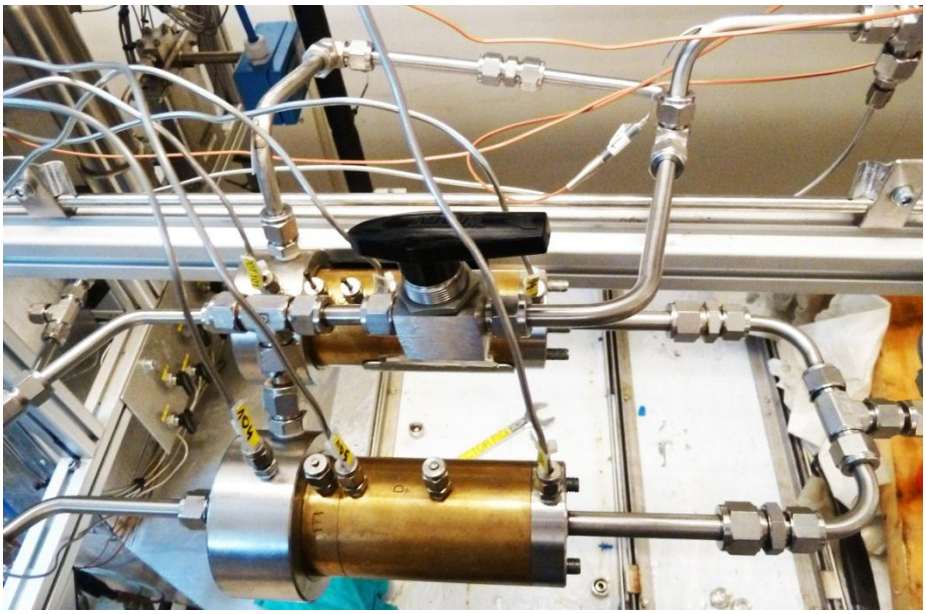

Figure 29: Photo of system modifications performed to investigate parallel ejector operation.

There were normally six pressure transmitters dedicated to measure pressures in ejector. To measure pressures in both installed ejectors, three indicators were disconnected from the main geometry and connected to the second one. Opened indicator sockets, which were not in use, has been closed with specially prepared caps. After this modification, pressures were measured in each of ejectors in three places, namely: motive nozzle inlet, mixing chamber inlet and diffuser outlet.

Before starting the system, vacuum pump was connected to the system for 1h. After evacuating all of air, the installation was filled up with CO_2 again. The last step before performing next tests was checking the leaks in the part of the system which was touched during modification process.

5.3.1. Investigation Methods for Experiment II

For the second test two measurement procedures were planned. To obtain the final results, just one was used. Following section briefly describes both procedures and explains the fact of choosing just one of them.

Geometries investigation method

First idea of testing the parallel operation, was to investigate the geometries itself to make a short characteristics of parallel ejectors set. The plan was to investigate first few measuring points for ejector P2GGC. The next step should be investigation of second ejector - A2CDC. At the end parallel work should be investigated and compared, to observe the effects of common operation. The most important assumption for those tests was to compare the three cases for the same conditions, namely: motive nozzle pressure and temperature, suction nozzle pressure and temperature, discharge pressure.

After preparing the system for investigation, several random tests were done. The measuring points were obtained by changing compressor speed as well as changing the temeperature levels for heat sources at gas cooler and evaporator. During comparison of the first results, it was certified that investigation of two different geometries and parallel work for the same inlet and outlet conditions is not possible on existing rig. The dependence between inlet and outlet boundaries is too sensitive. It is not able to obtain the same conditions for three different cases. For similar motive nozzle inlet conditions and suction nozzle inlet conditions, the outlet conditions are noticeably different. The reason of this performance is compressor presence in the installation. For obtaining desired parameters at the same level another type of system should be built, which is described in the Conclusions part. Table 8 shows the differences for random compared test results.

Table 8: Comparison of inlet and outlet conditions obtained in the first test method for parallel operation. (where: t_{mn} – temperature at the motive nozzle inlet, p_{mn} – pressure at the motive nozzle inlet, t_{sn} – temperature at the suction nozzle inlet, p_{sn} – pressure at the suction nozzle inlet, p_{out} – pressure at ejectors discharge)

Geometry	**t_{mn}, °C**	**p_{mn}, bar**	**t_{sn}, °C**	**p_{sn}, bar**	**p_{out}, bar**
P2GGC	34,7	80,71 bar	15,9	37,68	42,63
A2CDC	34,5	81,07 bar	15,4	37,34	39,81
Parallel Operation	34,8	81,15 bar	15,7	37,51	43,72

Fallowing investigation trial shows also very important fact for designing systems with parallel ejectors sets. The total mass flow rate of two ejectors working in parallel is not a sum of specific mass flow rates for separated ejectors working on the same inlet conditions. Fallowing Table 9 compares the values for one measurement:

Table 9: Comparison of mass flow rates for two different geometries and parallel operation of both. (where: t_{mn} – temperature at the motive nozzle inlet, p_{mn} – pressure at the motive nozzle inlet, t_{sn} – temperature at the suction nozzle inlet, p_{sn} – pressure at the suction nozzle inlet, p_{out} – pressure at ejectors discharge, m_{mn} – motive nozzle mass flow rate, m_{sn} – suction nozzle mass flow rate)

Geometry	**t_{mn}, °C**	**p_{mn}, bar**	**t_{sn}, °C**	**p_{sn}, bar**	**m_{mn}, kg/min**	**m_{sn}, kg/min**
P2GGC	34,7	80,71	15,9	37,68	3,12	0,83
A2CDC	34,5	81,07	15,4	37,34	1,87	0,45
Parallel Operation	34,8	81,15	15,7	37,51	4,44	1,52

System investigation method

Second idea of investigation, was to investigate how the parallel work of ejectors affects the system. The plan was to change the temperature of heat sources at the gas cooler for steady compressor speed and evaporator heat source temperature setpoint. The test should be repeated for P2GGC geometry, later for A2CDC geometry and in the end for both geometries working in parallel. Important fact is that the system investigation test heat exchanges were switched from tube-in-tube to plate heat exchangers, due the plate ones are equipped in temperature indicators installed in desired places, namely at inlet and outlet.

In the first try, the compressor speed was set up at 90% of maximum RPM to obtain high motive nozzle pressures. The temperature on evaporator heat source was set up at 20°C and the temperature on gas cooler heat source was varied between 25°C and 40°C, with 5°C step. It was not possible to finish the tests for chosen compressor speed. The reason were too low CO_2 pressures obtained for the suction nozzle of A2CDC geometry. Pressure for the evaporator should be maintained above 34 bar, since below this pressure system was freezing. It is because 34bar is the pressure level adequate for 0°C for CO_2. The fluid in evaporator heat source loop is water, which freezes below 0°C.

In the second try the compressor speed was decreased to 40% of maximum RPM. The temperature levels described before were repeated in this case. Reduction of compressor speed was a success. Pressures maintained for evaporation side were higher than 34 bar for all performed tests. Table 10 shows the settings for obtained measurements.

Table 10: System settings comparison for measurements performed in Experiment II.

Geometry	Compressor speed	Evaporator heat source temperature	Gas cooler heat source temperature
P2GGC	40% of maximum RPM	20°C	25°C
			30°C
			35°C
			40°C
A2CDC	40% of maximum RPM	20°C	25°C
			30°C
			35°C
			40°C
Parallel Operation	40% of maximum RPM	20°C	25°C
			30°C
			35°C
			40°C

5.3.2. Experiment II Calculations

For second experiment system calculations were performed. Most of the equations used to obtain the results for this part of investigation were presented in previous subchapters. Just few additional equations are presented here.

The important value calculated for the compressor is the shaft power. It is calculated using measured values of rotational speed and torque:

$$P_{shaft} = 2 \cdot \pi \cdot n_{comp} \cdot Tr \tag{46}$$

where: n_{comp} – rotational speed, Tr – torque.

Most important value in this part is the coefficient of performance (COP). Equations (47) and (48) shows the way of COP calculation for the heating and cooling unit :

$$COP = \frac{\dot{Q}_{gc}}{P_{shaft}} \tag{47}$$

$$COP = \frac{\dot{Q}_{ev}}{P_{shaft}} \tag{48}$$

where: $\dot{Q}_{gc}$ - gas cooler heat capacity, $\dot{Q}_{ev}$ - evaporator heat capacity.

5.3.3. Results of Experiment II

In second experiment 12 measuring points were obtained, according to system settings shown in the Table 9. Four points for P2GGC geometry, four for A2CDC geometry and four for parallel operation. In fallowing subsection the results of tests are presented as well as briefly discussed.

The first important comparison is performed to identify how the coefficient of performance depends on the different gas cooler heat source temperatures, which mainly simulates the varying ambient conditions for a refrigeration cycle. Figure 30 shows the dependence between described values for three different cases.

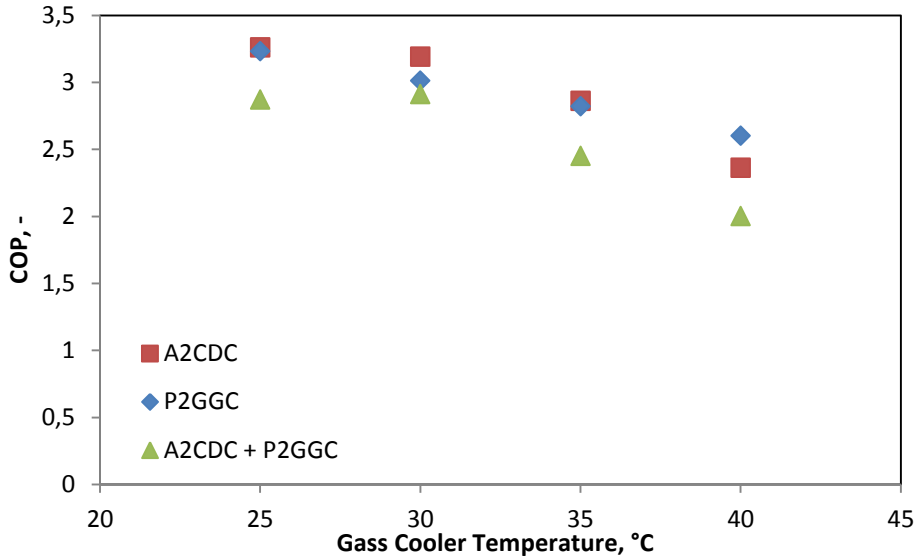

Figure 30: Dependence of COP in respect to gas cooler heat source temperature.

Analyzing the graph, it is clear that the parallel work of two different geometries chosen for the test is not an advantage for the system. The highest COP values are obtained for the A2CDC geometry, characterized by smaller motive nozzle diameter. The COP values for the case of parallel operation are lower than the COP values for single operation of P2GGC geometry, characterized by bigger motive nozzle diameter. It can not be said, that this kind of results will be obtained for other geometries sets. The reason of obtained values could be also testing geometries on the same compressor speed level, namely low one. In the further investigations compressor speed should be varied also, together with gas cooler heat source temperature.

In second comparison the dependence between calculated COP and gas cooler heating capacity is considered.

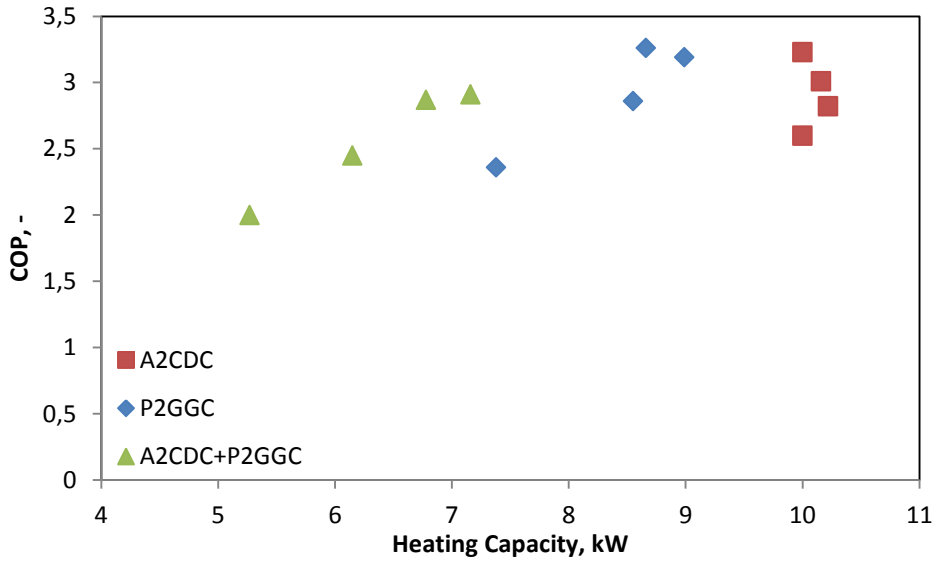

Figure 31: Dependence of COP in respect to calculated gas cooler heating capacity.

The graph shown on Figure 31 presents that the highest heating capacities are obtained again for the single operation of A2CDC ejector. The parallel operation gives again the lowest numbers.

The last comparison considers the dependence between ejector pressure lift and gas cooler heat source temperature. It shows the work of ejector in different ambient conditions.

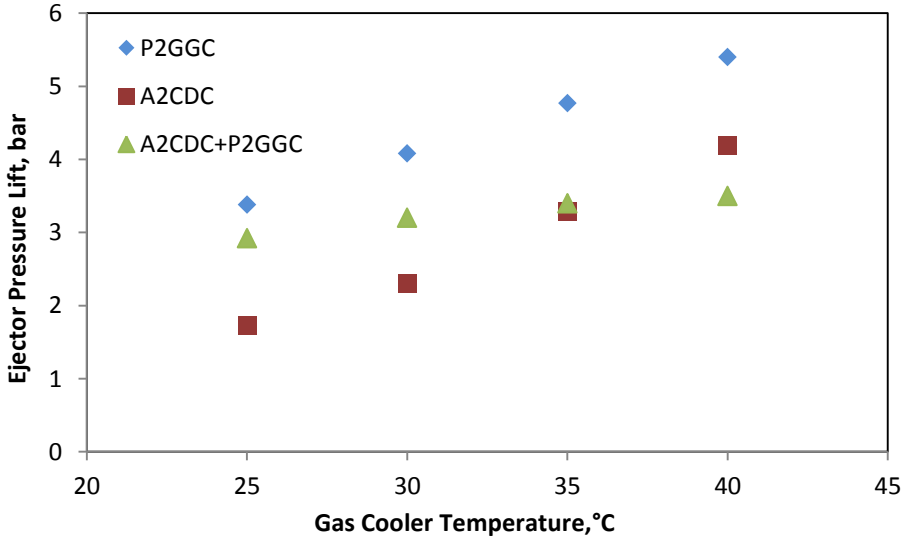

Figure 32: Dependence of ejector pressure lift in respect to gas cooler heat source temperature.

Figure 32 shows that pressure lift is increasing for the rising gas cooler heat source temperature. The higher numbers are obtained for P2GGC geometry. In the parallel operation case, the pressure lift does not depend that significant on the ambient conditions and it varies in a slight range. The lowest values are obtained for the A2CDC geometry, characterized by smaller motive nozzle diameter.

PART III

6 Conclusions

Investigations of transcritical R744 systems with applied ejectors are still desired. Tests performed in NTNU/SINTEF laboratories show the need of searching the optimal combination of ejectors geometries to investigate parallel ejector operation.

Feasibility Study

Performed feasibility study of conceptual R744 transcritical cycle with three different ejector geometries applied shows the need of building this kind of rig for the future tests. Different compressors sets could be used, which gives broader range to test different combinations of the ejector geometries, characterized by smaller as well as larger motive nozzle diameters. Testing three ejectors in parallel could give also interesting results of COP cycle values.

Single P2GGC operation

Testing the P2GGC geometry on the rig, gave a big number of results. Basing on this database, the characteristic of geometry was obtained. Created characteristic could be used in the further work. It can be implemented in such modeling language as Modelica, to simulate real ejector behavior in the system in which it could be implemented. However, created characteristic is not perfect. It is because most of the measuring points are in the same pressure range, which is giving accurate form of characteristic in this range, but for the other points the characteristic is just partial. To create better characteristic, the geometry should be tested in wider motive nozzle pressures range.

Parallel P2GGC and A2CDC operation

The most important part of investigation performed in NTNU/SINTEF laboratory is the test of parallel ejector operation. The idea was to create and compare partial characteristic of P2GGC and A2CDC geometries, and compare them to the partial characteristic of both working in parallel. This task could not be performed, because of the whole rig characteristic. All of the components are working in the same compressor loop. Therefore any changes set up on one in one place of the rig, are strongly effecting another measuring points. Facing this situation, it is not possible to obtain the same inlet and outlet

conditions of two different geometries, and compare with parallel ejectors set working in similar conditions. To perform this kind of tests and comparisons another type of rig should be considered. One of the ideas could be building a rig with two different geometries working in parallel and supplied by two separate and independent CO_2 bottles. For accurate values and performance factors, a feasibility study should be performed first.

Second part of parallel ejectors operation shows the results of use second ejector working in parallel. For chosen geometries set, namely A2CDC and P2GGC, there is no advantage obtained by using two ejectors in parallel. The COP factor values are lower than COP values for single ejectors. The reason of such results could be testing the parallel set in one compressor speed, namely very low. For future tests another geometries should be chosen also. Interesting test could be also investigation of two equal geometries working in parallel.

References

[1] Zha S. Report on investigation of ejector for CO2 transcritical system. Norwegian University of Science and Technology, Department of Energy and Process Engineering, Trondheim, Norway, 2008.

[2] Adamowicz P. Masters thesis, Faculty of Energy and Environmental Engineering, Application of Computer Sciences in Energy and Environmental Engineering, Silesian University of Technology, Investigation of different ejector geometries., Gliwice, Poland, 2010.

[3] Drescher M., Hafner A., and Banasiak K. Experimental parameter investigation of R744 ejector. In *8th IIR Gustav Lorentzen Conference on Natural Working Fluids*, Copenhagen, 2008.

[4] Elbel S. and Hrnjak P. Experimental validation of a prototype ejector designed to reduce throttling losses encountered in transcritical R744 system operation. *International Journal of Refrigeration*, **31**:411–422, 2008.

[5] Kohler J., Richter C., Tegethoff W., and Tischendorf W. Experimental and theoretical study of a CO2 ejector refrigeration cycle. In *VDAWinter meeting*, Saalfelden, 2007.

[6] Hafner A. *Compact interior heat exchangers for CO2 mobile heat pumping systems*. PhD thesis, Norwegian University of Science and Technology, Trondheim, Norway, 2003.

[7] Nehdi E., Kairouani L., and Bouzaina M. Performance analysis of the vapour compression cycle using ejector as an expander. *International Journal of Energy Research*, **31**:364–375, 2007.

[8] Lorentzen G. Revival of carbon dioxide as a refrigerant. *International Journal of Refrigeration*, **17**(5), 1994.

[9] www.ccohs.ca - Canadian Centre for Occupational Health and Safety.

[10] http://www.dorin.com/ - Official DORIN S.p.A. website.

[11] Szargut J., Termodynamika, PWN, Warszawa, 1980.

[12] Garzía-Valladares O., Pérez-Segarra C.D., Oliva A. Numerical simulation of capillary tube expansion devices behavior with pure and mixed refrigerants considering metastable region. Part I: Mathematical formulation and numerical model, Applied Thermal Engineering 22, p. 173-182, 2002.

[13] Feburie V., Goit M., Granger S., Seynhaeve J.M. A model for choked flow trough cracks with inlet subcooling, International Journal of Multiphase Flow 19 (4), p. 541 – 562, 1993.

[14] Rusinowski H. Diagnostyka cieplna eksploatacji w energetyce, Wydawnictwo Oddziału PAN w Katowicach, Gliwice-Katowice, 2010.

[15] Jurkowski A. Masters thesis, Experimental investigation of ejectors applied in R744 transcritical heat pumping system., Gliwice, Poland, 2011.

Appendix

1. Test facility starting procedure.

2. Test facility shutting off procedure.

3. CD with electronic copy of thesis.

1. For starting the system:

- Run the pumps in the water/glycol gas cooler and evaporator cycles.
- Turn on the cooling unit placed in the basement and the heater in the basement.
- Turn on the heaters in the water/glycol gas cooler and evaporator cycles.
- Initialize compressor by key in the blue box.
- Switch on the compressor control valve in the compressor panel.
- Click compressor initialize in the LabView control panel.
- Turn compressor on in LabView control panel.
- Control the amount of carbon dioxide load in the separator.
- Control by valves the oil mass flow at the liquid outlet of the separator and at the return from the compressor.
- Red lights in the LabView control panel indicate that the measurement device is outside range of operation.

2. For shutting off the system:

- Set up the compressor speed on minimal range in the LabView panel.
- Turn off the compressor using LabView.
- Turn off the compressor by key in the compressor control panel.
- Turn off the compressor control valve in compressor control panel
- Turn off heaters in the water/glycol gas cooler and evaporator cycles.
- Turn off the heater in the basement, then turn off the cooling unit.
- When the temperature in the water/glycol gas cooler and evaporator cycles fall to the desired level, turn off the pumps.
- In the case of problems turn off the entire test rig by using red button with 'NØDSTOPP' description, at the blue box over the compressor.